Journal Pre-proof

Design, synthesis, and biological evaluation of 5-((8-methoxy-2-methylquinolin-4-yl)amino)-1*H*-indole-2-carbohydrazide derivatives as novel Nur77 modulators

Baicun Li, Jie Yao, Kaiqiang Guo, Fengming He, Kun Chen, Zongxin Lin, Shunzhi Liu, Jiangang Huang, Qiaoqiong Wu, Meijuan Fang, Jinzhang Zeng, Zhen Wu

PII: S0223-5234(20)30580-8

DOI: https://doi.org/10.1016/j.ejmech.2020.112608

Reference: EJMECH 112608

To appear in: *European Journal of Medicinal Chemistry*

Received Date: 25 April 2020

Revised Date: 12 June 2020

Accepted Date: 19 June 2020

Please cite this article as: B. Li, J. Yao, K. Guo, F. He, K. Chen, Z. Lin, S. Liu, J. Huang, Q. Wu, M. Fang, J. Zeng, Z. Wu, Design, Synthesis, and Biological Evaluation of 5-((8-Methoxy-2-Methylquinolin-4-yl)Amino)-1*H*-Indole-2-Carbohydrazide Derivatives as Novel Nur77 Modulators, *European Journal of Medicinal Chemistry*, https://doi.org/10.1016/j.ejmech.2020.112608.

Synthesis, and Biological Evaluation of 5-((8-Methoxy-2-Methylquinolin-4-yl)Amino)-1*H*-Indole-2-Carbohydrazide Derivatives as Novel Nur77 Modulators

Baicun Li[1, 2, #], Jie Yao[1, #], Kaiqiang Guo[1,#], Fengming He[1], Kun Chen[1], Zongxin Lin[1], Shunzhi Liu[1], Jiangang Huang[1], Qiaoqiong Wu[1], Meijuan Fang[1,*], Jinzhang Zeng[1,*], Zhen Wu[1,*]

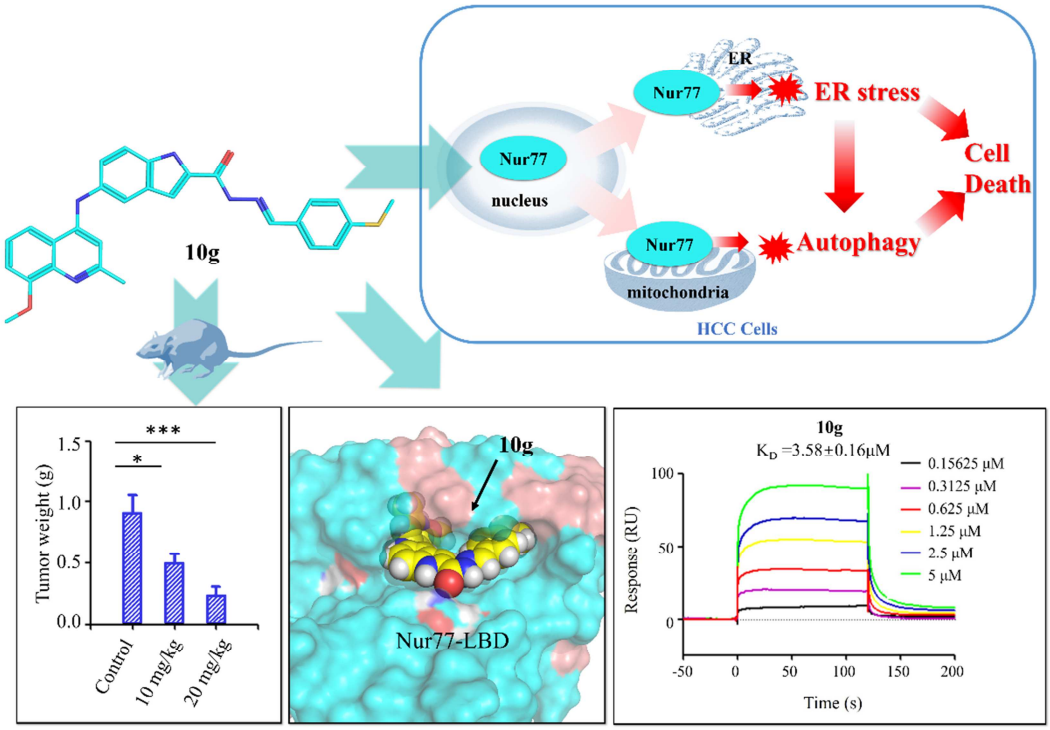

Novel Nur77 Modulator **10g** with anti-hepatoma activity, up-regulates Nur77 expression, mediates sub-cellular localization of Nur77, induces Nur77-dependent ER stress and autophagy, and results in cell apoptosis in HCC cells.

Design, Synthesis, and Biological Evaluation of 5-((8-Methoxy-2-Methylquinolin-4-yl)Amino)-1*H*-Indole-2-Carbohydrazide Derivatives as Novel Nur77 Modulators

Baicun Li[1, 2, #], Jie Yao[1, #], Kaiqiang Guo[1,#], Fengming He[1], Kun Chen[1], Zongxin Lin[1], Shunzhi Liu[1], Jiangang Huang[1], Qiaoqiong Wu[1], Meijuan Fang[1,*], Jinzhang Zeng[1,*], Zhen Wu[1,*]

[1] Fujian Provincial Key Laboratory of Innovative Drug Target Research and State Key Laboratory of Cellular Stress Biology, School of Pharmaceutical Sciences, Xiamen University, Xiamen 361102, China

[2] State Key Laboratory of Medical Molecular Biology, Department of Physiology, Institute of Basic Medical Sciences, Chinese Academy of Medical Sciences and School of Basic Medicine, Peking Union Medical College, Beijing 100005, China

[#]These authors contribute equally to this work

[*]Corresponding author. Fujian Provincial Key Laboratory of Innovative Drug Target Research and State Key Laboratory of Cellular Stress Biology, School of Pharmaceutical Sciences, Xiamen University, Xiamen 361102, China. *E-mail addresses:* fangmj@xmu.edu.cn (Meijuan Fang); jzzeng@xmu.edu.cn (Jinzhang Zeng), and wuzhen@xmu.edu.cn (Zhen Wu).

Abstract

Nur77 is a potential target for the treatment of cancer such as HCC. Herein, we detailed the discovery of a novel series of 5-((8-methoxy-2-methylquinolin-4-yl)amino)-1*H*-indole-2-carbohydrazide derivatives as potential Nur77 modulators. The studies of antiproliferative activity and Nur77-binding affinity of target compounds resulted in the discovery of a lead candidate (**10g**), which was a good Nur77 binder (K_D = 3.58±0.16 μM) with a broad-spectrum antiproliferative activity against all tested hepatoma cells (IC_{50} < 2.0 μM) and was low toxic to normal LO2 cells. **10g** could up-regulate Nur77 expression and mediate sub-cellular localization of Nur77 to induce apoptosis in hepatocellular carcinoma cell lines, which relied on **10g** inducing Nur77-dependent autophagy and endoplasmic reticulum stress as the upstream of apoptosis. Moreover, the *in vivo* assays verified that **10g** significantly inhibited xenograft tumor growth. These results indicate that **10g** has the potential to be developed as a novel Nur77-targeting anti-hepatoma drug.

Keywords: Nur77; quinoline; indole; antitumor; autophagy; ER stress.

1. Introduction

Hepatocellular carcinoma (HCC) is one of the most common cancer worldwide, which affects more than 700,000 patients every year[1, 2]. As HCC is a highly therapy-resistant cancer, the identification of new therapeutic targets and the development of small molecule drugs with the new structure and novel mechanism of action for HCC is necessary[3]. In a recent study, it was reported that Nur77 (also known as NR4A1, TR3 or NGFI-B) interacted with phosphoenolpyruvate carboxykinase (PEPCK1, the rate-limiting enzyme in gluconeogenesis) to increase gluconeogenesis and suppress glycolysis, resulting in suppression of HCC development[4]. Moreover, the UALCAN and Kalpen-Meier analyses based on the TCGA dataset show that Nur77 is expressed at a significantly lower level in cancer tissues than normal tissues in clinical samples **(Figure 1A&1B**). Kalpen-Meier survival plot shows that the high expression of Nur77 is positively correlated with overall survival (**Figure 1C**). Patients with high Nur77 expression tumors has significantly longer overall survival (OS) than those with low Nur77 expression tumors (**Figure 1C**). Additionally, it was widely reported that the nuclear receptor Nur77 could serve as a tumor suppressor for HCC[4, 5]. Therefore, the identification and optimization of small molecules which could upregulate the Nur77 level and activate the Nur77 function have emerged as a promising therapeutic strategy for HCC.

Insert Figure 1 here.

Figure 1. UALCAN and Kakaplan-meier analyses of Nur77 (NR4A1) in Hepatocellular carcinoma (LIHC). Box plot analysis of the immunoreactive score (IRS) of Nur77 (NR4A1) in 50 normal samples and 340 HCC samples grouped into stage I-IV with TCGA LIHC dataset(https://www.cancer.gov/). Nur77 expression is significantly down-regulated in LIHC. There are statistically significant differences in the expression level of Nur77 between normal tissues and tumor tissues of individual stages with a p-value less than 0.0001 (****) (**A**).

Expression profiling of Nur77 in the Kakaplan-meier plotter database. Nur77 expression is significantly lower in tumor tissues than in normal tissues. There are statistically significant differences in the expression level of Nur77 between tumor tissues and normal tissues with a p-value less than 0.05 (**B**). Kaplan-Meier survival curve shows the positive correlation between overall survival of HCC patients and Nur77 expression levels in 60 months from Kaplan-Meier Plotter dataset(http://kmplot.com/). Patients with Nur77 expression values below the 50th percentile are classified as lower Nur77 levels, while above the 50th percentile are classified as higher Nur77 levels. The median expression level was used as the cutoff. Survival information of 288 patients is available. HR (Hazards Ratio) =0.57, p(HR)=0.0022 (**C**).

Orphan nuclear receptor Nur77 plays an vital role in cell metabolism[6, 7], differentiation[8], proliferation, endoplasmic reticulum stress (ER stress)[9], apoptosis[10], and autophagy[11]. Nur77 expression and function depend on tumor type. As shown in **Figure S1**, Nur77 is overexpressed in a few types of tumors such as DLBC (diffuse large B-cell lymphoma), PAAD (pancreatic adenocarcinoma), and THYM (thymic carcinoma). However, Nur77 is notably underexpressed in the vast majority of tumor tissues (**Figure S1**), *e.g.* LIHC (liver hepatocellular carcinoma), BRCA (breast invasive carcinoma), LUAD (lung adenocarcinoma) and LUSC (lung squamous cell carcinoma). In these Nur77-underexpressed tumors, Nur77 could act as an anti-oncogene and display anti-tumor activity[4, 5]. The anti-tumor mechanisms of Nur77 may be involved in many ways and are not fully understood. During the past decades, many studies have demonstrated that Nur77 has the anti-tumor activity by inducing apoptosis not only in HCC, but also in prostate, lung, gastric, breast, and colon cancer cells[12-16]. Autophagy and endoplasmic-reticulum (ER) stress are important biological mechanisms for cells to maintain homeostasis and adapt to environmental stress[17]. It has been well documented that ER stress and autophagy dysfunction contribute to the initiation and development of cancer[18, 19]. On the other hand, for tumor cells, incomplete autophagy flux and unrestrained autophagy could result in cell death[20-22]. Nowadays, cancer therapies based on

autophagy targeted agents have distinctly attracted much attention. Interestingly, it has been found that Nur77 could interact with Nix to activate autophagy[11] or bind to p62 to participate in autophagy[23]. Additionally, ER stress-mediated cell death in a variety of diseases makes this process an attractive target for therapy[24]. ER stress could induce apoptosis through both mediating autophagy and the eIF2/ATF4/CHOP pathway[25]. It has also been proven that Nur77 can participate in ER stress to induce cell death[9]. However, the mechanism of Nur77 transport to mitochondria and endoplasmic reticulum participation in autophagy and endoplasmic reticulum stress has still not been fully revealed.

Due to the important effect of Nur77 in many cell biological processes, many chemical entities of various scaffolds have been identified or developed as Nur77 modulators in recent years. For example, Nur77 modulators with potent antitumor activity mainly include (**Figure 2**): 12-O-tetradecanoylphorbol-13-acetate (TPA)[26, 27], all-*trans* retinoic acid (ATRA)[27], 6-(3-(1-adamantyl)-4-hydroxyphenyl)-2-naphthalene carboxylic acid (CD437 or AHPN)[12], Celastrol[23], Cisplatin[28], Cytosporone B[29, 30], Fenretinide[31], *N*-butylidenephthalide[32-34], methylene-substituted diindolylmethanes (C-DIMs)[35], B-cell lymphoma-2 converting peptide (NuBCP-9)[36], 1-(2,4,6-trihydroxyphenyl)-1-nonanone (THPN)[11], paclitaxel[37], and Panobinostat[38], *etc*. Among them, THPN, Celastrol, and Cytosporon B can specifically bind to the Nur77-LBD (the ligand-binding domain of Nur77) for functional regulation[39]. However, there is no literature supporting on the direct modulation on Nur77 of cisplatin, paclitaxel, 12-O-tetradecanoylphorbol-13-acetate (TPA), Fenretinide, *N*-butylidene phthalide, Panobinostat, all-trans retinoic acid (ATRA), and CD437. Additionally, it has been documented that TPA[40], ATRA[40], *N*-butylidenephthalide[33], C-DIMs[35], NuBCP-9[36], and paclitaxel[37] can induce Nur77-mediated apoptosis. THPN and Celastrol might induce autophagy *via* Nur77 translocation to the mitochondria [11, 23]. CD437 and TPA can induce cancer cell death through Nur77 transport to the mitochondria and endoplasmic reticulum

(ER) [9, 40].

Insert Figure 2 here.

Figure 2. Chemical structures of representative Nur77 Regulators.

Natural and synthetic compounds containing quinoline or/and indole motifs boast a wide variety of biological activities such as anti-bacterial[41, 42], anti-cancer[43-45], anticonvulsant[46, 47], anti-inflammatory[48, 49], and cardiovascular activities[50, 51]. It has been implied that quinoline and indole are two important bioactive moieties for drug design[52, 53]. Moreover, some identified Nur77 modulators are with the structure of the indole ring (Panobinostat) or the quinoline bioisosteres such as naphthalene ring (CD437) and 3-hydroxynaphthalen-2(8H)-one (Celastrol). Thus, a series of 5-((8-methoxy-2-methylquinolin-4-yl)amino)-1*H*-indole-2-carbohydrazide derivatives as new Nur77 modulators were designed, synthesized, and screened for the antiproliferative activity and the direct binding ability with Nur77. The structure−activity relationships (SARs) of synthesized compounds for antiproliferative activity were elucidated. Compound **10g** was identified as the most potent binder of Nur77 which exhibited good anti-proliferative activity against liver cancer cell lines (HepG2, QGY-7703, and SMMC-7721), and low cytotoxic property in the liver normal cell line (LO2). Therefore, compound **10g** was further investigated for its molecular basis of anti-cancer activity as a good Nur77 binder. The bioassay data indicated that **10g** could upregulate the expression of Nur77 and translocation to ER and mitochondria, where it participated in ER stress and autophagy induction. Compound **10g** could induce Nur77-dependent endoplasmic reticulum stress *in vitro*, which triggered autophagy and apoptosis in hepatoma cells. The anti-tumor effect of **10g** was further verified in a nude mouse xenograft model. Herein, we reported the design, synthesis, and subsequent biological evaluation of

5-((8-methoxy-2-methylquinolin-4-yl)amino)-1*H*-indole-2-carbohydrazide derivatives as a new class of Nur77 modulators.

2. Results and Discussion

2.1. Chemistry

2.1.1 Structure-based drug design

In the present study, the structure-based rational drug design was used to look for a new class of Nur77-targeting compounds with potent antitumor activities. We first used the SiteMap[54] suite in Schrödinger software to explore and analyze the surface of Nur77-LBD (PDB ID: 4RE8), to identify all potential small-molecules binding sites. Notably, the top-ranked site with a SiteScore and Dscore of 1.003 and 1.006, respectively, was composed of the co-crystal ligand (**3mj**) binding subsite (S') and a hydrophobic adjacent cavity (S''), exhibiting a U-shape structure **(Figure 3A** & **3B)**. The native ligand **3mj** (a direct Nur77-modulator, **Figure S2**) was the initial compound to design novel chemical entities targeting Nur77. Simultaneously, as CD437 and Panobinostat could well bind to the pocket of Nur77-LBD in molecular docking simulation (**Figure S3** & **Table S1**), the two compounds were selected as the leading compounds for the design of new Nur77-targeting compounds in the present study. CD437 contains a naphthalene ring which is a quinoline bioisostere, while Panobinostat has an indole ring. Herein, considering that the inclusion of the indole and quinoline moieties might contribute to the anticancer potency and Nur77-targeting binding potency, the benzene ring of **3mj** was changed into a rigid binary ring (the quinoline group), on which the indole moiety was further introduced. Taken together, we used the scaffold replacement and molecular hybridization strategies, leading to constructing the 5-((8-methoxy-2-methylquinolin-4-yl)amino)-1*H*-indole core as the new Nur77 modulators' scaffold. Subsequently, to obtain the "U-shape" molecules, together with consideration to synthetic accessibility, the C-2 position of indole ring was extended

via a linker (carbohydrazide) by another aromatic ring (R) holding or not holding substituents (**Figure 3C**). The aromatic ring R with or without substituent groups are described in **Figure 3D**, which were supposed to interact with the small hydrophobic pocket (S'' subsite).

Insert Figure 3 here.

Figure 3. Design strategies used in our present study to obtain novel Nur77 regulators with 5-((8-methoxy-2-methylquinolin-4-yl)amino)-1*H*-indole scaffold

Next, to confirm the rationality of this structure-based design, the molecular docking simulations between target compounds and Nur77-LBD were performed to evaluate the binding affinities of protein-ligand complexes, by using SP Glide of Schrödinger with default settings. The Glide docking scores of most target compounds with Nur77-LBD were range from -4.799 to -7.788, while the native ligand 3mj had a docking score of -5.021. The docking results indicated that most of the target compounds had moderate binding affinities with Nur77-LBD. Among them, **10g** (SP mode, docking score = -4.967) was selected as a representative compound for further analysis (**Figure S4 & S5**). To gain more details on the interaction mode of **10g** and Nur77-LBD, we further performed Induced Fit docking simulations on **10g** and Nur77-LBD (**Figure S6**). **Figure 3E** and **3F** showed the docked pose of **10g** in the "U-shape" binding site of Nur77-LBD (docking score = -10.531, IFD Score = -509.43). As depicted in **Figure 3F,** 5-((8-methoxy-2-methylquinolin-4-yl)amino)-1*H*-indole moiety of **10g** was oriented toward the larger hydrophobic pocket (S' subsite), with an additional H-bond occurring between the amine hydrogen atom and carboxyl moiety of Glu114 which reinforced this binding conformation. The 4-(methylthio)phenyl moiety bound into the small hydrophobic pocket (S'' subsite) and formed hydrophobic interactions with Leu204, Val208, Leu221, and Cys220. Beyond these, the oxygen atom of the carbohydrazide linker also showed a hydrogen bond contact with the residue of

Gln197. Moreover, we used MM-GBSA module integrated in Schrödinger to calculate ΔG_{bind}values of Nur77-3mj complex and Nur77-**10g** complex obtained from Induce Fit docking. Compared with the native ligand **3mj (**ΔG_{bind}= -78.31 kcal/mol**)**, **10g** (ΔG_{bind}= -143.61 kcal/mol) showed a higher binding affinity to Nur77. These results suggested that target compounds including **10g** had the potentials to be Nur77 binders.

The molecular docking study demonstrated that 5-((8-methoxy-2-methylquinolin-4-yl)amino)-1*H*-indole-2-carbohydrazide was the promising scaffold of novel Nur77 modulators for further examination. Therefore, a total of 35 derivatives of 5-((8-methoxy-2-methylquinolin-4-yl)amino)-1*H*-indole-2-carbohydrazide **(Scheme 1 & Table 1)** were synthesized accordingly. All compounds were evaluated for the antiproliferative effects **(Table 1)** and Nur77-binding affinities **(Figure S8)**. After a preliminary screening, the most outstanding compound **10g** was further investigated, including the activities of the control of Nur77 expression, cell cycle arrest, apoptosis-inducing, autophagy-inducing, and ER stress-inducing activities in hepatoma carcinoma cells, and inhibition of tumor growth in a mouse hepatoma xenograft model.

2.1.2. Compound synthesis

The target compounds **10a-10z** and **10A-10I** were synthesized according to the synthetic route outlined in **Scheme 1**. (4-nitrophenyl) hydrazine **1** were refluxed with ethyl pyruvate in ethanol to afford compound **2** and then underwent ring closure with the presence of polyphosphoric acid to give ethyl 5-nitro-1*H*-indole-2-carboxylate **3**. Reduction of the nitro group of **3** with Fe in acetic acid aqueous obtained the key intermediate, ethyl 5-amino-1*H*-indole-2-carboxylate **4**. Meanwhile, the reaction of 2-methoxyaniline **5** with ethyl acetoacetate under polyphosphoric acid condition provided 8-methoxy-2-methylquinolin-4-ol **6**, followed by chlorination using $POCl_3$ to get the other key intermediate **7** (4-chloro-8-methoxy-2-methylquinoline). Then,

N-alkylation reaction of **4** with **7** gave ethyl 5-((8-methoxy-2-methylquinolin-4-yl)amino)-1*H*-indole-2-carboxylate (**8**), followed by refluxing with hydrazine hydrate in ethanol to get 5-((8-methoxy-2-methylquinolin-4-yl)amino)-1*H*-indole-2-carbohydrazide (**9**). Finally, target compounds (**10a-10z** and **10A-10I**) were prepared *via* reactions between **9** and corresponding aldehydes in refluxing ethanol.

The chemical structures of target compounds were characterized by ESI-MS, HRMS, ^{1}H NMR, and ^{13}C NMR. Moreover, these acylhydrazone compounds (**10a-10z** and **10A-10I**) were further identified as a single *E*-isomer according to our previous work[55] and other similar studies[56-59] .

Insert Scheme 1 here.

Scheme 1. Preparation of target compounds **10a-10z** and **10A-10I**. Reaction conditions: (a) Ethyl pyruvate, ethanol, reflux; (b) Polyphosphoric acid, 100□, 2 h; (c) Fe, acetic acid aqueous, 70□, 2 h; (d) Polyphosphoric acid, ethyl acetoacetate, 120□; (e) $POCl_3$, 130□; (f) 1-Butanol, concentrated hydrochloric acid**,** reflux; (g) hydrazine hydrate, ethanol, reflux; (h) ethanol, substituted aldehydes, trifluoroacetic acid, reflux.

2.2. Biological evaluation

2.2.1. In vitro antiproliferative activity

All the target compounds in this study were evaluated for the antiproliferative activities against three human hepatoma cell lines (HepG2 cells, QGY-7703 cells, and SMMC-7721 cells) and one normal hepatocyte line (LO2) using MTT assay with Celastrol (PC1), CD437 (PC2), and Cisplatin (PC3) as references. As shown in **Table 1,** most target compounds with the different aromatic groups introduced at the *N′*-methylene position, exhibited moderate antiproliferative activity against at least one test cancer cell line, with IC_{50} value below 10.0 μM. According to these data, the

preliminary structure-activity relationships (SARs) of these novel 5-((8-methoxy-2-methylquinolin-4-yl)amino)-1*H*-indole-2-carbohydrazide derivatives were summarized.

Insert Table 1 here.

Table 1. *In vitro* antiproliferative activities of target compounds against liver cancer and normal cells

(i)The influence of substitutes of the phenyl ring

When the moiety R was the *ortho* mono-substituted phenyl groups, compounds with 2-fluoro (**10a**), 2-chloro (**10b**), and 2-methoxy (**10c**) substitutions, exhibited excellent antiproliferative activities against all the four tested cell lines including three cancer cell lines and one normal cancer cell line. When the moiety R was the *meta* or *para* mono-substituted phenyl groups (**10d-10j**), the type of substituted groups played a pivotal role in antiproliferative profiles. Compound **10d** (R=3-methylpheny) had a broad spectrum of antiproliferative activities against both tumor and normal cells. However, compounds **10e-10j** showed low antiproliferative activity against at least one cell line. For example, the replacement of 3-CH_3 with 3-OCH_3 (**10d** *vs* **10e**), resulted in significantly decreased antiproliferative activity in both HepG2 and QGY-7703 cell lines with the IC_{50} value of higher than 20.00 μM. The conversion of 3-CH_3 to 3-CF_3 (**10d** *vs* **10f**) led to a sharp decreased antiproliferative inhibition on SMMC-7721, but no obvious influence in HepG2 and QGY-7703 cell lines. Inspiringly, compound **10g** showed potent anti-proliferative activities (IC_{50} < 5.0 μM) against all three liver cancer lines (HepG2, QGY-7703, and SMMC-7721), and low cytotoxic property in liver normal cells (LO2). Interestingly, changing the methoxy group (**10h**) to methylthio (**10g**) led to a significant difference in activity (**Table 1** & **Figure S7**), which might result from the different binding

affinities of **10h** and **10g** with Nur77 (**Table S2** & **Figure S7**).

In the target compounds **10k**-**10z** which contain di- or tri- substituted phenyl ring (R), the types and substituted positions of substitutes displayed an important relationship with the antiproliferative activity. Compounds with 2,3-dimethoxy (**10k**), 2,4-dimethoxy (**10l**), 2,3,4-trimethoxy (**10x**), and 4-methoxy-3-trifluoromethyl (**10r**) substituted phenyl groups had good antiproliferative activities against all tested cancer and normal cells. However, compounds with 2,5-dihydroxy (**10m**), 3,4-dimethoxy (**10n**), 3,5-dimethoxy (**10w**), and 3,4,5-trimethoxy (**10y**) substituted phenyl groups showed poor cytotoxicity profiles against all the four cell lines. In addition, substitution of nitro group (**10p**) and trifluoromethyl group (**10t**) at the C-4 position of phenyl ring had remarkably lowered the cytotoxicity (IC_{50} **>** 20.0 μM), implying that substitution of electron-withdrawing groups at phenyl ring was unhelpful for antiproliferative activity.

(ii) The influence of different aromatic R groups

Compounds **10B** and **10F** which had 2-thiopheneyl and 4-methoxynaphthalen-1-yl moieties, respectively, retained good antiproliferative activities for all tested cell lines (IC_{50}, 1.0–17.0 μM). However, compounds with 1*H*-pyrrole-2-yl (**10A**), 3-pyridyl (**10D**), and 4-pyridyl (**10E**) moieties displayed a dramatic decrease in the cellular antiproliferative activity. Quinoline-4-yl (**10G**), 2-chloroquinoline-3-yl (**10H**), and 5-methoxy-2-methyl-1*H*-indole-3-yl (**10I**) groups introduced at the *N*′-methylene position had low toxic to LO2 cells but caused a narrow spectrum antiproliferative activity against hepatoma cells.

Taken together, cell proliferation assay demonstrated that most of the target compounds exhibited moderate anticancer activity, preferably mono-substitution on phenyl ring. Among them, **10g** displayed potent and broad-spectrum antiproliferative activity against all tested three hepatoma cell lines (HepG2, QGY-7703, and SMMC-7721), and less cytotoxicity against LO2 cells (human normal liver cell line).

These results suggested that **10g** had the potential to become a safer candidate for antitumor drugs.

*2.2.2. **10g** can bind to Nur77 in vitro*

Nur77 is an attractive target for the treatment of HCC, we'd like to discover new anticancer agents targeting Nur77. Thereby, all target compounds were evaluated for the binding ability with Nur77-LBD using a single concentration binding assay by surface plasmon resonance (SPR) technology-based experiment **(Figure S8)**. Importantly, the SPR experiment showed that the introduction of mono-substituted phenyl ring at the carbon atom of hydrazine group (C=N) is more beneficial for the binding activity with Nur77 compared with other substituted aryl ring. When tested at 10.0 μM concentration, compounds **10h**, **10g**, and **10r** could well bind to Nur77 with RU values of 88.202, 91.587, and 90.948, respectively. Among these three compounds, both **10g** and **10r** showed potent and broad-spectrum antiproliferative activity against all tested hepatoma cells, with IC_{50} values of less than 2.0 μM, but only **10g** did not show significant cytotoxicity against liver normal cells (LO2) at the tested concentrations **(Table 1)**. The above assays showed that **10g** had low cytotoxic property, a broad spectrum antiproliferative activity against hepatoma cells, and a potent binding affinity to Nur77. As the lack of selectivity between normal and cancer cells is one of the main limitations of anticancer drugs, **10g** was selected for further study.

To confirm the physical binding ability of **10g** with Nur77-LBD, the SPR assay, and fluorescence ligand binding assay were performed. The SPR results showed that **10g** dose-dependently bound to Nur77-LBD with a K_D (equilibrium dissociation constant) value of 3.58±0.16 μM, and exhibited fast association/dissection kinetics to interact with Nur77-LBD (**Figure 4A**). The effect of **10g** on Nur77-LBD fluorescence intensity was shown in **Figure 4B**. There was a strong fluorescence emission of Nur77-LBD peaked at 332 nm (excitation at 280 nm). When a fixed concentration of Nur77-LBD was titrated with different concentrations of **10g**, a

remarkable intrinsic fluorescence decrease of Nur77-LBD was observed. The calculated K_D value from the fluorescence ligand binding assay was 1.34±0.19 μM. Together, these results demonstrated that **10g** could directly and efficiently bind to Nur77-LBD *in vitro*.

Insert Figure 4 here.

Figure 4. 10g bound to Nur77-LBD *in vitro*. Characterization of the binding affinity between **10g** and Nur77-LBD by the SPR assay (**A**). Fluorescence titration curve of Nur77-LBD with **10g**. The concentration of **10g** increased from 0.2 μM to 4 μM at an interval of 0.2 μM (**B**).

*2.2.3. **10g** regulates Nur77 expression at the cellular level*

In all tested hepatocellular carcinoma cell lines, **10g** could up-regulate the expression of Nur77 in a dose-dependent manner (**Figure 5A**). In HepG2 cells, the expression of Nur77 peaked after the treatment of **10g** for 6 h, while the expression of other nuclear receptors including RXRα and RARγ didn't significantly change (**Figure 5B**). This suggested that **10g** might specifically regulate the expression of Nur77. However, the mechanism by which Nur77 rapidly degraded after induction is not well understood[60, 61]. It has been reported that the half-life of Nur77 is extremely short, being about 20 to 40 min[62]. This may lead to a gradual decline in Nur77 levels after 6 hours of **10g** treatment.

In recent years, various non-genomic actions of Nur77 have been discovered, which are closely related to cell survival[63]. The antitumor activity of Nur77 was largely based on its extranuclear non-genomic action, so we investigated whether **10g** caused the extranuclear transport of Nur77 by using immunofluorescence experiments. As shown in **Figure 5C**, there were a large number of translocations of Nur77 into the cytoplasm from the nucleus when HepG2 cells were treated with **10g** for 6 h. The results of western blotting analyses also showed that the amount of Nur77 in cytoplasm increased, while that in the nucleus decreased with time increasing (**Figure 5D**).

Furthermore, confocal microscopy analysis revealed that **10g** promoted extensive mitochondrial translocation of endogenous Nur77 (**Figure 5E**). Endogenous Nur77 was also recorded for its translocation to the endoplasmic reticulum from the cell nucleus, when cells were treated with **10g** (**Figure 5F**). These results demonstrated that **10g** could promote the high expression and subcellular translocation of Nur77.

Insert Figure 5 here.

Figure 5. **10g** regulated the expression and sub-cellular translocation of Nur77. HepG2, QGY-7703, and SMMC-7721 cells treated with the indicated concentration of **10g** for 6 hours were analyzed for Nur77 by western blotting, GAPDH was used as an internal control (**A**). HepG2 cells were treated with 2.0 μM **10g** for the indicated time. The expression of Nur77, RXRα, and RARγ were detected by western blotting (**B**). Fluorescent images of HepG2 cells treated with 2.0 μM **10g** for indicated time and detected by Nur77. The nuclei were stained with DAPI. Scale bar, 10 μm (**C**). HepG2 cells were treated with 2.0 μM **10g** for the indicated time. Nur77 was detected in the cytoplasm and nuclear by western blotting. PARP was used as an internal control of the nucleus and Tubulin was used as an internal control of cytoplasm (**D**). HepG2 cells were treated with 2.0 μM **10g** for 6 hours and then incubated with the Nur77 antibody and Mito-tracker (**E**) or ER tracker (**F**). Scale bar, 10 μm.

*2.2.4. Nur77-dependent antitumor mechanism of **10g** in HCC cell lines*

*2.2.4.1. Growth inhibition of hepatoma carcinoma cells by **10g***

To evaluate the effect of **10g** on cell viability and cell proliferation, MTT assay and colony formation were performed. The results indicated that **10g** reduced the viability of HepG2, QGY-7703, and SMMC-7721 in a time-dependent manner (**Figure 6A**). The inhibitory effect of **10g** in HepG2, QGY-7703, or SMMC-7721 was also evaluated by using the crystal violet exclusion assay. It showed that the colony formation units

decreased significantly with the treatment of **10g** (**Figure 6B**). In HepG2 cells, phase-contrast micrograph experiments revealed that **10g** induced cell morphology alteration, such as cell shrinkage, vesicles accumulated, and reduced cell number (**Figure 6C**). These data suggest that **10g** has significant *in vitro* inhibitory effects on hepatoma cells.

Insert Figure 6 here.

Figure 6. 10g inhibited the growth and proliferation of HCC. HepG2, QGY-7703, and SMMC-7721 cells were treated with 2.0 μM **10g** with the indicated time. Cell viability was determined by MTT assays (**A**). The number of colonies was counted after the treatment of HepG2, QGY-7703, and SMMC-7721 cells with DMSO or 2.0 μM **10g** (**B**). HepG2 cells were treated with **10g** at the indicated concentrations, and the morphological changes were observed by optical microscopy at the indicated time (**C**).

*2.2.4.2. **10g** induces Nur77-dependent apoptosis*

To examine whether the growth inhibition of cancer cells induced by **10g** was associated with apoptosis, we checked the level of the cleaved PARP (c-PARP, a marker for apoptosis) in hepatoma cells treated with or without **10g**. The level of the cleaved PARP was increased with the increasing concentrations of **10g** treatment in HepG2, QGY-7703, and SMMC-7721 cells (**Figure 7A**). Additionally, Annexin V-FITC/PI assay showed that early and late phase apoptosis cells increased from 34.6% to 91.3% in HepG2, with an increase of **10g** concentration from 1.0 to 2.0 μM (**Figure 7B**). To verify whether **10g** could induce Nur77-dependent apoptosis, the Nur77 knockdown (shNur77) HepG2 cells were employed. Firstly, the c-PARP reversed obviously in shNur77 HepG2 cells treated with **10g** (**Figure 7C**). Furthermore, early and late phase apoptosis cells with 2.0 μM **10g** treatment were reduced from 80.5% to 40.0%, with Nur77 knocking down (**Figure 7D**). The decrease of mitochondrial membrane potential is a landmark event in the early stage of apoptosis. The decrease of cell membrane potential is easily detected by the

transformation of JC-1 from red fluorescence to green fluorescence, which is being used as a detection indicator of early apoptosis. So we further examined the effect of **10g** on the cell membrane potential using JC-1 staining (**Figure 7E**). When HepG2 cells were treated with 2.0 μM **10g**, the median intensity of green fluorescence of JC-1 increased from 41669 to 71731 units, while the median intensity of red fluorescence of JC-1 decreased from 23598 to 10298 units. However, there were no significant changes in shNur77 HepG2 cells. Collectively, these results suggest that the **10g** inducing cell apoptosis is dependent on Nur77.

To explore whether the apoptosis induced by 10g was caused by the nuclear exudation of Nur77, HepG2 cells were pretreated with or without 20 nM leptomycin B (LMB, an inhibitor of nuclear export) and then exposed to **10g** for an additional 12 hours. Finally, we checked the translocation of Nur77 by fluorescent microscope and examined the protein levels of PARP and Nur77 using Western blotting analysis. As shown in **Figure S9A**, LMB could hinder Nur77 nuclear exudation induced by **10g**. Moreover, LMB inhibited the **10g** induced apoptosis of HepG2 cells without affecting the Nur77 expression (**Figure S9B**). On the other hand, overexpression of Nur77 did not cause the death of HepG2 cells (**Figure S9C**). Collectively, these results suggest that the **10g** inducing cell apoptosis is dependent on Nur77 translocation.

Insert Figure 7 here.

Figure 7. 10g induced Nur77-dependent apoptosis. Western blot analysis of proteins involved in apoptosis after treatment with **10g** at the indicated concentrations for 12 hours in HepG2, QGY-7703, and SMMC-7721 cells (**A**). Annexin V/PI staining of HepG2 cells treated with **10g** at the indicated concentrations for 12 hours and assessed by flow cytometry (**B**). HepG2 or shNur77 HepG2 cells were treated with 2.0 μM **10g** for 12 hours. Cells were then subjected to Western blotting for PARP cleavage and Nur77 detecting (**C**), Annexin V/PI staining for apoptosis measurement (**D**), and JC-1 staining for mitochondrial membrane potential assay (**E**).

*2.2.4.3. **10g** induces Nur77-dependent autophagy*

Autophagy plays a dual role in tumor cell metabolism. On one hand, under the condition of nutrient deprivation, tumor cells maintain their survival through autophagy. On the other hand, autophagy is a way to promote cell death. Some anti-tumor drugs induce autophagy to cause the death of tumor cells. Beclin1 plays an important role in the formation of phagocytes in the early stage of autophagy. Meanwhile, the microtubule-associated protein 1 light chain 3 (LC3) is a widely recognized biological marker of autophagy[64]. LC3 protein expression level will be enhanced, and LC3-I will be transformed into LC3-II during autophagosome maturation with the participation of various ATG proteins. P62/SQSTM1 is a ligand-protein for LC3 binding, which is responsible for the degradation of ubiquitinated aggregates in autophagosomes. Furthermore, p62 can induce complete autophagy after binding to LC3 and is excessively expressed upon the activation of autophagy[65].

Nowadays, it has been reported that Nur77 can activate autophagy[11]. Herein, LC3-II and Beclin1 protein levels were first determined in HepG2, QGY-7703 and SMMC-7721 cells treated with or without **10g** for 12 h. It was observed that LC3-II and Beclin1 protein levels increased after **10g** treatment in a dose-dependent manner (**Figure 8A**). The most widely used method for autophagy detection is the observation and quantification of GFP-LC3 puncta by fluorescence microscopy. To verify **10g**'s ability in autophagy induction, HepG2 cells transfected with the GFP-LC3 were treated with or without 2.0 μM **10g** for 6 h and GFP-LC3 puncta in HepG2 cells was then checked by fluorescence microscopy. As depicted in **Figure 8B,** GFP-LC3 puncta were observed in cells treated with **10g** but not in control cells. However, GFP-LC3 puncta were not located in the vesicles. Surprisingly, **10g** treatment did not enhance p62 degradation, indicating that autophagy induced by **10g** was incomplete (**Figure S10**). These data imply that **10g** can cause autophagy in

HCC cells.

To further explore whether **10g** induced autophagy was related to Nur77, LC3, and Beclin1 expression levels were checked in the scramble control group (scr) and Nur77-knockdown group (shNur77) HepG2 cells treated with or without 2.0 μM **10g** for 6 or 12 h. Beclin1 expression level had no significant difference between normal and Nur77-knockdown HepG2 cells, but LC3 expression level decreased in Nur77-knockdown HepG2 cells (**Figure 8C**). Besides, HepG2 and shNur77 HepG2 cells both transfected with GFP-LC3 were treated 2.0 μM **10g** for 6 h, and then GFP-LC3 were examined by fluorescence microscopy. As shown in **Figure 8D**, GFP-LC3 puncta in wild-type HepG2 cells treated with **10g** displayed a dramatic increase, while slightly increased in Nur77-knockdown HepG2 cells. We also found that LC3-II expression slightly increased in Nur77 overexpressed HepG2 cells with **10g** treatment (**Figure S11**). Taken together, these results suggest that **10g** inducing incomplete autophagy in HCC cells is dependent on Nur77 to some content.

Insert Figure 8 here.

Figure 8. Induction of autophagy by **10g** in HCC. HepG2, QGY-7703 and SMMC-7721 were treated with **10g** at the indicated concentrations for 12 h, the levels of LC3 and Beclin1 were detected by Western blotting (**A**). Phase-contrast and fluorescent images of HepG2 cells transfected with GFP-LC3 and treated with 2.0 μM **10g** for 6 hours. Scale bar, 10 μm (**B**). HepG2 or shNur77 HepG2 cells were treated with DMSO or 2.0 μM **10g** for 6 hours or 12 hours. Cells were then subjected to Western blotting for LC3, Beclin1, and Nur77 detecting (**C**). Fluorescent images of HepG2 and shNur77 HepG2 cells transfected with GFP-LC3 and treated with 2.0 μM **10g** for 6 hours. Scale bar, 10 μm (**D**).

*2.2.4.4. **10g** induces Nur77-dependent ER stress*

ER stress is caused by abnormal accumulation of proteins in the endoplasmic

reticulum. ER stress might affect various stress responses of cells, such as injury, autophagy, and apoptosis. Bip protein, as a member of heat shock protein 70, is located in the endoplasmic reticulum cavity to assist the transfer of the newly formed protein into the internal reticulum. As a target molecule of endoplasmic reticulum stress, Bip accumulates when the endoplasmic reticulum occurs. CHOP and TRB3, as response genes to ER stress, are highly expressed after ER stress, causing cell biological behaviors such as apoptosis and autophagy. TRB3 is a downstream gene of CHOP[66].

Nur77 could participate in ER stress to induce cell death, so we checked whether **10g** caused ER stress in hepatocellular carcinoma cells. As shown in **Figure 9A**, the expression of endoplasmic reticulum stress-related proteins including Bip, CHOP, and TRB3 was dose-dependently increased in all three HCC cell lines with the treatment of **10g** for 12 h. In line with this observation, immunostaining of the ER luminal marker protein disulfide isomerase (PDI) showed a striking dilation in the ER of **10g**-treated HepG2 cells (**Figure 9B**). To clarify whether **10g** mediate Nur77-dependent ER stress, HepG2 and shNur77 HepG2 cells were treated with or without 2.0 μM **10g** for 6 or 12 h, and then the expression levels of Bip, CHOP, and TRB3 were analyzed by western blot (**Figure 9C**). It showed that there was a significant decrease in the expression of Bip and CHOP in shNur77 HepG2 cells, compared to HepG2 cells treated with **10g**. Meanwhile, we observed that the expression levels of TRB3 both in HepG2 and shNur77 HepG2 cells were decreased at 12 h, while Bip expression level was slightly increased with the increased treated time of **10g**. Simultaneously, immunostaining showed PDI dots in shNur77 HepG2 cells treated with **10g** were less than in wild-type HepG2 cells treated with **10g** (**Figure 9D**). These results reveal that **10g** inducing ER stress is in Nur77 dependent manner.

Insert Figure 9 here.

Figure 9. Induction of ER stress by **10g** in HCC. HepG2, QGY-7703 and SMMC-7721 were treated with **10g** at the indicated concentrations for 12 h, the levels of Bip, TRB3, and CHOP were detected by western blotting (**A**). Phase-contrast and fluorescent images of HepG2 cells and treated with 2.0 μM **10g** for 6 hours and then incubated with PDI antibody. Scale bar, 10 μm (**B**). HepG2 or shNur77 HepG2 cells were treated with DMSO or 2.0 μM **10g** for 6 hours and 12 hours. Cells were then subjected to Western blotting for TRB3, Bip, CHOP, and Nur77 detecting (**C**). Fluorescent images of HepG2 and shNur77 HepG2 treated with 2.0 μM **10g** for 6 hours and then incubated with PDI antibody. Scale bar, 10 μm (**D**).

*2.2.4.5. **10g** induces ER stress-mediated autophagy and autophagy-dependent cell apoptosis*

We then investigated the relationship of autophagy, ER stress, and cell apoptosis, which were induced by **10g**. HepG2 cells were treated with 2.0 μM **10g** for the indicated time. The expression of Nur77 began to rise after **10g** treatment for one hour and reached the peak at 6 hours. The expression of Bip, p-EIF2a, and TRB3 increased at one to four hours. Subsequently, LC3 II expression began to increase in 4-6 hours. Finally, PARP was significantly cleaved after 6 hours (**Figure 10A**). To further investigate whether autophagy and ER stress were contributed to **10g**-induced cell death, we combined **10g** with the autophagy inhibitor 3-MA or the ER stress inhibitor 4-PBA to treat HepG2 cells. Once autophagy and ER stress were inhibited, PARP cleavage, Caspase-3 cleavage, and caspase-9 cleavage induced by **10g** were reduced and the ratio of Bax/Bcl2 was also decreased (**Figure 10B** and **10C**). Interestingly, when HepG2 cells were treated with **10g** and 4-PBA at the same time, the expression level of LC3-II was significantly weakened (**Figure 10C**), implying that **10g**-induced ER stress could promote autophagy.

Taken together, it suggests that **10g** can induce cell apoptosis through ER stress and autophagy pathways.

Insert Figure 10 here.

Figure 10. 10g induced apoptosis-dependent autophagic cell death mediated by ER-stress. HepG2 cells were treated with 2.0 μM **10g** for indicated time. The levels of autophagy associated proteins, ER stress-associated proteins, and Nur77 were detected by Western blotting (**A**). HepG2 cells were pretreated with 3-MA (2.0 mM) for 2 hours prior to exposure to **10g** for an additional 12 hours. Western blotting was performed to examine the changes in protein levels of PARP, cleaved-caspase-3, cleaved-caspase-9, Bcl-2, Bax, Bip, and LC3(**B**). HepG2 cells were pretreated with 4-PBA (2.0 mM) for 2 hours prior to exposure to **10g** for an additional 12 hours. Western blotting was performed to examine the levels of PARP, cleaved-caspase-3, cleaved-caspase-9, Bcl-2, Bax, Bip, EIF2a, TRB3, and LC3(**C**).

*2.2.5. The antitumor activities of **10g** in vivo*

To evaluate the *in vivo* antitumor potency of **10g**, we established a mice hepatoma HepG2 xenograft model. **10g** was administered once every day for 15 days (10 mg/kg/day *i.p.* and 20 mg/kg/day *i.p.*), and the tumor sizes were measured every day. After the experiment was completed, the mice were sacrificed to strip the tumors and organ tissues, the body weight and stripped tumors were weighted, and the safety and effectiveness of **10g** were evaluated by hematoxylin and eosin (H&E) staining and immunohistochemistry analysis.

As shown in **Figure 11**, **10g** treatment could lead to substantial suppression of tumor growth (**Figure 11A**), the tumor growth inhibition (TGI) values at doses of 10 mg/kg/day and 20 mg/kg/day were 36.74 % and 62.38 %, respectively (**Figure 11C**). The average tumor weights of drug treatment groups were 0.24 ± 0.13 g (20 mg/kg/day, *i.p.*) and 0.50 ± 0.15 g (10 mg/kg/day, *i.p.*), which were significantly lower than control group (0.86 ± 0.18 g) (**Figure 11B**). The results shown in **Figure 11C** indicated that **10g** exhibited almost no influence on the body weight of experimental mice, while it significantly suppressed tumor weight, indicating its safe usage. Furthermore, immunohistochemistry analysis showed that cells of the tumor tissue in the drug groups were sparser and vacuolated than the control group (**Figure**

11D). Immunostaining and Western blotting of tumor tissues prepared from non-treated and treated mice revealed that the expression level of proliferation marker PCNA was markedly reduced by **10g** (**Figure 11E&F**). Together, these results demonstrate that **10g** inhibits tumor growth with good tolerability *in vivo*.

We also determined the autophagy and ER stress effect of **10g** in animals. Immunostaining and western blotting analyses of tumor tissues showed that compared with the control group, the administration groups exhibited significantly increased expressions of Nur77, autophagy (LC3, Beclin1) and ER stress (TRB3, Bip, CHOP) markers (**Figure 11E&F**). Furthermore, the translocation of Nur77 in the cytoplasm was also observed in the high dose treatment group (**Figure 11F**). These results further suggest that **10g** potently induces autophagy and ER stress in a xenograft mouse model of HepG2 cells, which is consistent with the cellular results.

Insert Figure 11 here.

Figure 11. 10g exhibited antitumor efficacy in a xenograft mouse model of HepG2 cells. Nude mice (n=15) injected with HepG2 (5×10^6 cells) were administrated with the indicated dose of **10g** (10 mg/kg, *i.p.*; 20 mg/kg, *i.p.*) once a day and tumors were measured every day. 15 days after administration of **10g**, nude mice were sacrificed and tumors were removed, weighted and showed (***P< 0.001, **P< 0.01, *P< 0.05) (**A, B**). Tumor volume and body weight of nude mice during treatment (***P< 0.001, **P< 0.01, *P< 0.05, ·P< 0.05) (**C**). H&E staining in tumors after 15 days of treatment with **10g** (**D**). Micromagnification was 200, 400, and 1000 times respectively. Immunocytochemistry staining showing the expression of Nur77, PCNA, LC3, Beclin1, TRB3, Bip, and CHOP in tumor tissues prepared from nude mice treated with or without **10g** (10 mg/kg; 20 mg/kg) for 15 days (**E**). Western blot analysis of the expressions of Nur77, PCNA, LC3, Beclin1, TRB3, Bip, and CHOP in tumor tissues prepared from nude mice treated with or without **10g** (10 mg/kg, *i.p.*; 20 mg/kg, *i.p.*) for 15 days (**F**).

3. Conclusion

In summary, we presented the successful design and synthesis of a new class of 5-((8-methoxy-2-methylquinolin-4-yl)amino)-1*H*-indole-2-carbohydrazide derivatives as potent Nur77 modulators. One of the lead compounds of this class, **10g**, was identified as a Nur77-specific modulator with a broad-spectrum inhibition on hepatoma cells and low toxic. **10g** exhibited cellular Nur77-targeted anticancer mechanism of action. The apoptosis, autophagy, and ER stress inductions of **10g** were in a Nur77-dependent manner. Moreover, further mechanistic experiments revealed that **10g**-induced ER stress led to the activation of incomplete autophagy and promoted the apoptotic death of tumor cells. Taken altogether, **10g** might be a promising candidate for further development into a chemotherapeutic agent for the treatment of HCC.

4. Experimental section

4.1. Chemistry

The commonly used reagents were purchased from Beijing Innochem Technology Co., Ltd. and used without further purification. The melting points (mp) were determined using a Shanghai Jingke SGW X-4 microscope melting point apparatus. Thin-layer chromatography (TLC, silica gel HSGF254, Yantai Jiangyou Silicone Development Co., Ltd. (Yantai, Shandong, China)) was used to monitor for completeness of the reaction visualized by UV light (λ=254 nm or λ=365 nm). And the obtained compounds were purified by silica gel column chromatography. ^{1}H NMR and ^{13}C NMR were carried out using the Bruker Avance III spectrometer at 600 MHz for ^{1}H NMR and 150 MHz for ^{13}C NMR spectrophotometer, (Faculty of Pharmacy, Xiamen University, Fujian, China), at 25□ in DMSO-d6 using tetramethylsilane (TMS) as an internal standard and chemical shifts were recorded in ppm on the δ scale using DMSO-d6 (2.5) as a solvent. Coupling constant (J) values were estimated in Hertz (Hz). Splitting patterns are designated as follows: s, singlet; br s, broad singlet;

d, doublet; t, triplet; q, quartet; dd, doublet of doublet; m, multiplet. Mass spectra were measured on an LCMS-2020 Single Quadrupole Mass Spectrometer (Shimadzu). And the HR-ESI-MS analysis was performed on the Thermo Q-Exactive Mass spectrometer (Thermo Fisher Scientific Corporation, Waltham, Massachusetts, USA) equipped with electrospray ionization source (ESI).

*4.1.1. Ethyl (Z)-2-(2-(4-nitrophenyl)hydrazineylidene)propanoate **2***

To a stirred solution of (4-nitrophenyl)hydrazine **1** (10.0 g, 65.0 mmol) in anhydrous ethanol (85 mL), ethyl pyruvate (8.1 g, 72.0 mmol) was added dropwise at room temperature. After completion of the dropwise addition, the mixture was heated at reflux for 2 hours. The reaction was cooled to room temperature, filtered under suction, and washed with ethanol to give compound **2** (13.8 g). Yellow solid, yield 89.6%, mp: 197-199□; ^{1}H-NMR (600 MHz, $CDCl_3$): δ8.21 (d, *J*=9.0 Hz, 2H), 8.09 (s, 1H), 7.28 (d, *J*= 9.0 Hz, 2H), 4.32-4.39 (m, 2H), 2.17(s, 3H), 1.40 (t, *J*= 7.1 Hz, 3H); ESI-MS(+): *m/z* 252.1 $[M+H]^+$.

*4.1.2. Ethyl 5-nitro-1H-indole-2-carboxylate **3***

Compound **2** (10.0 g, 42.0 mmol) and polyphosphoric acid (110.0 g) were added into a dry 500 mL round-bottom flask. The reaction mixture was heated to 100°C under stirring for 2 hours. The reaction solution was cooled to room temperature and poured into 200 mL of ice water. Then, the mixture was filtered, and the filter cake was collected and dried to give compound **3** (9.5 g). Green solid, yield: 90.2%; ^{1}H-NMR (600 MHz, DMSO-d6): δ12.58 (br s, 1H), 8.71 (d, *J*= 2.0 Hz, 1H), 8.12 (dd, *J*= 2.2, 9.2 Hz, 1H), 7.61 (d, *J*= 9.2 Hz, 1H), 7.42 (d, *J*= 1.0 Hz, 1H), 4.37 (q, *J*= 7.1 Hz, 2H), 1.35 (t, *J*= 7.2 Hz, 3H); ESI-MS(+): *m/z* 235.0 $[M+H]^+$.

*4.1.3. Ethyl 5-amino-1H-indole-2-carboxylate **4***

Ethanol (80 mL), water (20 mL), acetic acid (10 mL), reduced iron powder (8.6 g, 154.0 mmol) were added in a dry 250 mL round bottom flask and stirred under 75°C for half an hour to activate the iron powder. Then, compounds **3** (9.0 g, 39.0 mmol)

was added to the reaction mixture and heated to 75°C under stirring for 2 hours. The reaction solution was filtered while hot, and the filtrate was removed under vacuum. The resulting mixture was added with 80 mL of water and 80 mL of ethyl acetate. The pH of the mixture was adjusted to around 7.5 with sodium bicarbonate solution and then filtered. The organic layer was separated from the aqueous layer, dried with anhydrous sodium sulfate (15 g) for 8 h, filtered, and concentrated in vacuo to provide the crude product, which was purified by silica gel column chromatography (petroleum ether: ethyl acetate = 3:1, *v/v*) to afford compound **4** (6.1 g). Yellowish solid, yield: 77.7% ; ^{1}H-NMR (600 MHz, DMSO-d6): δ 11.38 (br s, 1H), 7.16-7.19 (m, 1H), 6.84 (dd, *J* = 0.8, 2.1 Hz, 1H), 6.69-6.73 (m, 2H), 4.63 (br s, 2H), 4.29 (q, *J*=7.1Hz, 2H),1.31 (t, *J*=7.2 Hz, 3H); ^{13}C-NMR (150 MHz, DMSO-d6): δ 161.9,142.5, 132.0, 128.2, 127.1, 117.2, 113.2, 106.6, 103.6, 60.6, 14.8; ESI-MS(+): *m/z* 205.0 $[M+H]^+$.

*4.1.4. 8-methoxy-2-methylquinolin-4-ol **6***

2-Methoxyaniline **5** (2.46 g, 20.0 mmol), ethyl acetoacetate (2.60 g, 20.0 mmol), polyphosphoric acid (70 g) were added to a dry 100 mL three-necked flask, respectively. The reaction was carried out at 120°C for 5 hours. The mixture was poured into 100 mL of ice water, stirred until completely dissolved, and cooled to room temperature. The pH of the mixture was adjusted to around 7.5 with the 30% sodium hydroxide solution, cooled to room temperature, and filtered. The filter cake was washed with water and dried to give compound **6** (3.70 g). White solid, yield 97.4%; ^{1}H NMR (600 MHz, DMSO-d_6): δ 11.11 (br s, 1H), 7.60-7.62 (m, 1H), 7.22 (d, *J* = 4.2 Hz, 1H), 7.21 (s, 1H), 5.95 (s, 1H), 3.97 (s, 3H), 2.37 (s, 3H); ESI-MS(+): *m/z* 190.0 $[M+H]^+$.

*4.1.5. 4-chloro-8-methoxy-2-methylquinoline **7***

A mixture of 8-methoxy-2-methylquinolin-4-ol **6** (1.89 g, 10 mol) and phosphorus oxychloride (20 mL) was added to the drying 100 mL pressure bottle. The reaction was stirred at 130□ for 4 hours. After the completion of the reaction, the

mixture was cooled to room temperature, removed the solvent under vacuum, added 50 mL of cold water, and decolorized by activated carbon. The filtrate was adjusted pH to around 8.5 with 10% NaOH under ice bath, filtered to give compound **7** (1.26 g). White solid, yield 60.9%. ESI-MS(+): *m/z* 208.0 $[M+H]^+$.

*4.1.6.Ethyl 5-((8-methoxy-2-methylquinolin-4-yl)amino)-1H-indole-2-carboxylate **8***

The mixture of 4-chloro-8-methoxy-2-methylquinoline **7** (41.0 mg, 20.0 mmol) and intermediates **4** (1.1 eq) in a 25 mL round bottom flask was refluxed in 1-butanol (8 mL) for 7 hours. The reaction was concentrated under vacuum to remove solvent to give the crude product, which was purified by silica gel column chromatography (DCM: MeOH = 20:1, *v/v*) to afford compound **8** (61 mg). Yellow solid, yield: 81.3%; ESI-MS(+): *m/z* 376.1 $[M+H]^+$.

*4.1.7. 5-((8-methoxy-2-methylquinolin-4-yl)amino)-1H-indole-2-carbohydrazide **9***

In a dry 100 mL round bottom flask, compound **8** (3.75 g, 10.0 mmol) and hydrazine hydrate (20 mL) were added into ethanol (20 mL). The mixture was refluxed for 10 hours. The reaction mixture was sufficiently cooled and filtered. The filter cake was washed with 20 mL of ice water and dried to give compound **9** (2.20 g). White solid, yield 61.1%; ESI-MS (+): *m/z* 362.5 $[M+H]^+$.

*4.1.8. General procedures for the synthesis of **10a-z** and **10A-I***

Compound **9** (72.0 mg, 0.2 mmol) was refluxed with different aldehyde (0.2 mol) in absolute ethanol (5 mL) containing two drops of trifluoroacetic acid for 8 hours. Then, the solvent was removed under reduced pressure at 40-45□ to give the crude product, which was purified by column chromatography to produce the corresponding 5-((8-methoxy-2-methylquinolin-4-yl)amino)-1*H*-indole-2-carbohydrazide derivatives (**10a-z and 10A-I).**

*4.1.8.1.(E)-N'-(2-fluorobenzylidene)-5-((8-methoxy-2-methylquinolin-4-yl)amino)-1H-indole-2-carbohydrazide (**10a**).* Orange solid (82.0 mg, 87.8%), mp: 228-230□. ^{1}H NMR (600 MHz, DMSO-d_6): δ 12.20 (br s, 1H), 12.16 (br s, 1H), 10.72 (s, 1H), 8.73

(br s, 1H), 8.21 (d, *J* = 8.4 Hz, 1H), 7.99 (t, *J* = 7.2 Hz, 1H), 7.81 (br s, 1H), 7.65-7.72 (m, 2H), 7.57 (d, *J* = 7.9 Hz, 1H), 7.49-7.55 (m, 1H), 7.46 (br s, 1H), 7.31-7.36 (m, 2H), 7.29 (dd, *J* = 2.0, 8.6 Hz, 1H), 6.57 (s, 1H), 4.12 (s, 3H), 2.59 (s, 3H); ^{13}C NMR (151 MHz, DMSO-d_6): δ 160.4, 158.4, 158.2, 157.9, 155.6, 154.7, 149.4, 136.4, 131.9, 130.0, 129.9, 128.0, 127.1, 126.8, 125.5, 123.0, 119.8, 117.2, 116.8, 116.6, 114.5, 114.4, 113.2, 104.6, 101.0, 57.2, 20.4; HRMS-ESI(+): *m/z* 468.1831 $[M+H]^+$, calcd for $C_{27}H_{23}FN_5O_2^+$ 468.1830.

*4.1.8.2.(E)-N'-(2-chlorobenzylidene)-5-((8-methoxy-2-methylquinolin-4-yl)amino)-1H-indole-2-carbohydrazide (**10b**).* Yellowish solid (67.0 mg, 69.4%), mp: 241-243□. ^{1}H NMR (600 MHz, DMSO-d_6): δ 12.27 (br s, 1H), 12.17 (br s, 1H), 10.71 (s, 1H), 8.89 (br s, 1H), 8.21 (d, *J* = 8.4 Hz, 1H), 8.07 (d, *J* = 5.9 Hz, 1H), 7.81 (s, 1H), 7.68-7.72 (m, 1H), 7.66 (d, *J* = 8.4 Hz, 1H), 7.55-7.59 (m, 2H), 7.45-7.50 (m, 3H), 7.29 (dd, *J* = 2.0, 8.6 Hz, 1H), 6.57 (s, 1H), 4.12 (s, 3H), 2.58 (s, 3H); ^{13}C NMR (151 MHz, DMSO-d_6): δ 158.3, 158.1, 157.9, 155.6, 154.7, 149.4, 143.7, 136.4, 133.7, 132.0, 130.5, 130.0, 129.9, 128.2, 127.4, 127.2, 123.0, 119.8, 118.9, 117.2, 114.5, 114.4, 113.2, 104.7, 101.1, 57.2, 20.4; HRMS-ESI(+): *m/z* 484.1536, 486.1507 $[M+H]^+$, calcd for $C_{27}H_{23}ClN_5O_2^+$ 484.1535, 486.1506.

*4.1.8.3.(E)-5-((8-methoxy-2-methylquinolin-4-yl)amino)-N'-(2-methoxybenzylidene)-1H-indole-2-carbohydrazide (**10c**).* Yellowish solid (56.0 mg, 58.5%), mp: 243-245□. ^{1}H NMR (600 MHz, DMSO-d_6): δ 12.11 (br s, 1H), 12.02 (s, 1H), 10.71 (s, 1H), 8.83 (s, 1H), 8.21 (d, *J* = 8.4 Hz, 1H), 7.91 (d, *J* = 7.3 Hz, 1H), 7.79 (s, 1H), 7.67-7.73 (m, 1H), 7.65 (d, *J* = 8.4 Hz, 1H), 7.57 (d, *J* = 7.9 Hz, 1H), 7.41-7.48 (m, 2H), 7.27 (dd, *J* = 1.9, 8.7 Hz, 1H), 7.14 (d, *J* = 8.3 Hz, 1H), 7.05 (t, *J* = 7.5 Hz, 1H), 6.56 (s, 1H), 4.12 (s, 3H), 3.90 (s, 3H), 2.58 (s, 3H); ^{13}C NMR (151 MHz, DMSO-d_6): δ 158.3, 158.2, 157.7, 155.6, 154.7, 149.4, 143.3, 136.3, 132.1, 130.0, 129.8, 128.1, 127.2, 126.0, 122.8, 122.7, 121.3, 119.7, 117.2, 114.5, 114.4, 113.2, 112.4, 104.3, 101.0, 57.2, 56.2, 20.4; HRMS-ESI(+): *m/z* 480.2032 $[M+H]^+$, calcd for $C_{28}H_{26}N_5O_3^+$ 480.2030.

4.1.8.4.(E)-5-((8-methoxy-2-methylquinolin-4-yl)amino)-N'-(3-methylbenzylidene)-1H

*-indole-2-carbohydrazide (**10d**).* Yellow solid (40.0 mg, 43.2%), mp: 196-198□. ^{1}H NMR (600 MHz, DMSO-d_6): δ 12.13 (br s, 1H), 12.03 (s, 1H), 10.72 (s, 1H), 8.45 (s, 1H), 8.21 (d, *J* = 8.3 Hz, 1H), 7.8 (br s, 1H), 7.64-7.72 (m, 2H), 7.53-7.60 (m, 3H), 7.44 (br s, 1H), 7.37 (t, *J* = 7.6 Hz, 1H), 7.28 (dd, *J* = 2.0, 8.6 Hz, 2H), 6.57 (s, 1H), 4.12 (s, 3H), 2.58 (s, 3H), 2.38 (s, 3H); ^{13}C NMR (151 MHz, DMSO-d_6): δ 161.2, 158.4, 158.2, 157.8, 155.6, 154.7, 149.4, 148.0, 138.6, 136.0, 134.7, 132.1, 130.0, 129.3, 128.1, 127.2, 122.4, 119.7, 119.4, 117.2, 116.7, 114.5, 114.4, 113.3, 101.0, 57.2, 21.4, 20.4; HRMS-ESI(+): *m/z* 464.2083 $[M+H]^+$, calcd for $C_{28}H_{26}N_5O_2^+$ 464.2081.

*4.1.8.5.(E)-5-((8-methoxy-2-methylquinolin-4-yl)amino)-N'-(3-methoxybenzylidene)-1 H-indole-2-carbohydrazide (**10e**).* Yellow solid (34.0 mg, 35.5%), mp: 211-213□. ^{1}H NMR (600 MHz, DMSO-d_6): δ 12.12 (br s, 1H), 12.07 (br s, 1H), 10.72 (s, 1H), 8.47 (s, 1H), 8.21 (d, *J* = 8.4 Hz, 1H), 7.79 (br s, 1H), 7.68-7.72 (m, 1H), 7.66 (d, *J* = 8.6 Hz, 1H), 7.57 (d, *J* = 7. 9 Hz, 1H), 7.45 (br s, 1H), 7.38-7.42 (m, 1H), 7.30-7.34 (m, 2H), 7.27-7.30 (m, 1H), 7.01-7.06 (m, 1H), 6.57 (s, 1H), 4.12 (s, 3H), 3.83 (s, 3H), 2.58 (s, 3H); ^{13}C NMR (151 MHz, DMSO-d_6): δ 160.0, 155.6, 154.7, 149.4, 147.9, 136.4, 136.2, 132.0, 130.5, 130.0, 129.8, 128.0, 127.1, 122.9, 120.5, 119.7, 118.9, 117.2, 116.7, 114.5, 114.4, 113.2, 111.8, 104.5, 101.0, 57.2, 55.7, 20.4; HRMS-ESI(+): *m/z* 480.2031 $[M+H]^+$, calcd for $C_{28}H_{26}N_5O_3^+$ 480.2030.

*4.1.8.6.(E)-5-((8-methoxy-2-methylquinolin-4-yl)amino)-N'-(3-(trifluoromethyl) benzylidene)-1H-indole-2-carbohydrazide (**10f**).* Yellow solid (41.0 mg, 39.7%), mp: 207-209□. ^{1}H NMR (600 MHz, DMSO-d_6): δ 12.22 (br s, 1H), 12.07 (br s, 1H), 8.56 (br s, 1H), 8.11 (s, 1H), 8.08 (d, *J* = 8.4 Hz, 2H), 7.82 (d, *J* = 7. 9 Hz, 1H), 7.71-7.76 (m, 2H), 7.63 (d, *J* = 8.6 Hz, 1H), 7.54 (t, *J* = 8.2 Hz, 1H), 7.43 (br s, 1H), 7.36 (d, *J* = 7. 9 Hz, 1H), 7.28 (dd, *J* = 2.0, 8.6 Hz, 1H), 6.56 (s, 1H), 4.03 (s, 3H), 2.49 (s, 3H); ^{13}C NMR (151 MHz, DMSO-d_6): δ 158.4, 158.2, 158.1, 155.9, 153.2, 147.8, 146.0, 136.0, 131.6, 130.6, 130.2, 130.0, 128.0, 126.8, 125.8, 125.4, 123.6, 123.4, 123.1, 118.9, 118.1, 116.8, 114.2, 111.3, 104.6, 101.1, 56.6, 22.7; HRMS-ESI(+): *m/z* 518.1797 $[M+H]^+$, calcd for $C_{28}H_{23}F_3N_5O_2^+$ 518.1798.

*4.1.8.7.(E)-5-((8-methoxy-2-methylquinolin-4-yl)amino)-N'-(4-(methylthio) benzylidene)-1H-indole-2-carbohydrazide (**10g**).* Yellow solid (81.0 mg, 81.8%), mp: 203-205□. ^{1}H NMR (600 MHz, DMSO-d_6): δ 12.13 (br s, 1H), 12.02 (s, 1H), 10.72 (s, 1H), 8.45 (s, 1H), 8.21 (d, *J* = 8.4 Hz, 1H), 7.76-7.81 (m, 1H), 7.70 (td, *J* = 4.2, 8.0 Hz, 3H), 7.66 (d, *J* = 8.6 Hz, 1H), 7.57 (d, *J* = 7. 9 Hz, 1H), 7.44 (br s, 1H), 7.34-7.37 (m, 2H), 7.28 (dd, *J* = 2.0, 8.6 Hz, 1H), 6.57 (s, 1H), 4.12 (s, 3H), 2.58 (s, 3H), 2.53 (s, 3H); ^{13}C NMR (151 MHz, DMSO-d_6): δ 158.3, 158.1, 155.6, 154.7, 149.4, 147.5, 141.5, 132.1, 131.2, 130.0, 129.1, 128.1, 128.0, 127.1, 126.1, 125.9, 122.8, 117.2, 114.5, 114.4, 113.2, 104.4, 101.0, 57.2, 20.4, 14.7; HRMS-ESI(+): *m/z* 496.1802 $[M+H]^+$, calcd for $C_{28}H_{26}N_5O_2S^+$ 496.1803.

*4.1.8.8.(E)-5-((8-methoxy-2-methylquinolin-4-yl)amino)-N'-(4-methoxybenzylidene)-1 H-indole-2-carbohydrazide (**10h**).* Yellow solid (77.0 mg, 80.4%). ^{1}H NMR (600 MHz, DMSO-d_6): δ 12.11 (br s, 1H), 11.93 (s, 1H), 10.71 (s, 1H), 8.44 (s, 1H), 8.21 (d, *J* = 8.6 Hz, 1H), 7.78 (br s, 1H), 7.68 - 7.73 (m, 3H), 7.65 (d, *J* = 8.6 Hz, 1H), 7.57 (d, *J* = 8.1 Hz, 1H), 7.42 (br s, 1H), 7.27 (dd, *J* = 1.8, 8.6 Hz, 1H), 7.05 (d, *J* = 8.8 Hz, 2H), 6.57 (s, 1H), 4.11 (s, 3H), 3.83 (s, 3H), 2.58 (s, 3H); ^{13}C NMR (151 MHz, DMSO-d_6): δ 161.3, 158.3, 157.7, 155.6, 154.7, 149.4, 147.8, 136.3, 132.2, 130.1, 129.8, 129.2, 128.1, 127.3, 127.1, 119.6, 117.2, 114.8, 114.5, 114.4, 113.2, 104.2, 101.0, 57.2, 55.8, 20.4; HRMS-ESI(+): *m/z* 480.2031 $[M+H]^+$, calcd for $C_{28}H_{26}N_5O_3^+$ 480.2030.

*4.1.8.9.(E)-N'-(4-cyanobenzylidene)-5-((8-methoxy-2-methylquinolin-4-yl)amino)-1H-indole-2-carbohydrazide (**10i**).* Yellow solid (47.4 mg, 50.0%), mp: 244-246□. ^{1}H NMR (600 MHz, DMSO-d_6): δ 12.07-12.15 (m, 1H), 11.36 (s, 1H), 10.73 (s, 1H), 10.08 (s, 1H), 8.56 (s, 1H), 8.21 (d, *J* = 8.6 Hz, 1H), 7.79 (s, 1H), 7.67-7.72 (m, 1H), 7.66 (d, *J* = 8.6 Hz, 1H), 7.56 (d, *J* = 7. 9 Hz, 1H), 7.41 (s, 1H), 7.36 (d, *J* = 8.4 Hz, 1H), 7.28 (dd, *J* = 2.0, 8.6 Hz, 1H), 6.57 (s, 1H), 6.39 (dd, *J* = 2.2, 8.4 Hz, 1H), 6.36 (d, *J* = 2.0 Hz, 1H), 4.11 (s, 3H), 2.59 (s, 3H); ^{13}C NMR (151 MHz, DMSO-d_6): δ 161.3, 159.8, 157.3, 155.6, 154.7, 149.4, 136.3, 131.9, 131.4, 130.0, 129.8, 128.1, 127.1, 122.8, 119.7, 117.2, 114.5, 114.4, 113.2, 111.1, 108.3, 104.3, 103.1, 101.0, 57.2,

20.4; HRMS-ESI(+): *m/z* 475.1878 $[M+H]^+$, calcd for $C_{28}H_{23}N_6O_2^+$ 475.1877.

*4.1.8.10.(E)-N'-(4-hydroxybenzylidene)-5-((8-methoxy-2-methylquinolin-4-yl)amino)-1H-indole-2-carbohydrazide (**10j**).* Yellow solid (17.0 mg, 18.3%). ^{1}H NMR (600 MHz, DMSO-d_6): δ 11.95 (br s, 1H), 11.78 (s, 1H), 8.37 (s, 1H), 8.01 (d, *J* = 8.3 Hz, 1H), 7.65-7.69 (m, 1H), 7.56-7.62 (m, 3H), 7.47 (t, *J* = 8.2 Hz, 1H), 7.34 (s, 1H), 7.27 (d, *J* = 7.7 Hz, 1H), 7.24 (dd, *J* = 2.0, 8.6 Hz, 1H), 6.87 (d, *J* = 8.6 Hz, 2H), 6.54 (s, 1H), 3.99 (s, 3H), 2.42-2.46 (m, 3H); ^{13}C NMR (151 MHz, DMSO-d_6): δ 161.4, 159.9, 157.7, 156.4, 148.1, 135.5, 135.1, 132.1, 131.9, 129.3, 128.2, 128.1, 125.7, 125.1, 122.8, 122.2, 118.4, 116.2, 114.0, 113.9, 113.8, 110.4, 103.8, 102.4, 101.1, 93.2, 56.4; HRMS-ESI(+): *m/z* 466.1874 $[M+H]^+$, calcd for $C_{27}H_{24}N_5O_3^+$ 466.1874.

*4.1.8.11.(E)-N'-(2,3-dimethoxybenzylidene)-5-((8-methoxy-2-methylquinolin-4-yl)amino)-1H-indole-2-carbohydrazide (**10k**).* Yellow solid (36.0 mg, 35.4%), mp: 237-239□. ^{1}H NMR (600 MHz, DMSO-d_6): δ 12.13 (br s, 1H), 12.07 (s, 1H), 10.69 (br s, 1H), 8.76 (s, 1H), 8.21 (d, *J* = 8.4 Hz, 1H), 7.79 (s, 1H), 7.67-7.73 (m, 1H), 7.66 (d, *J* = 8.6 Hz, 1H), 7.57 (d, *J* = 7. 9 Hz, 1H), 7.51 (d, *J* = 6.6 Hz, 1H), 7.45 (br s, 1H), 7.28 (dd, *J* = 2.0, 8.6 Hz, 1H), 7.12-7.18 (m, 2H), 6.57 (s, 1H), 4.11 (s, 3H), 3.86 (s, 3H), 3.83 (s, 3H), 2.56 - 2.61 (m, 3H); ^{13}C NMR (151 MHz, DMSO-d_6): δ 158.3, 158.1, 155.5, 154.8, 153.2, 149.5, 148.5, 143.4, 136.3, 132.1, 130.1, 129.9, 128.2, 128.1, 127.1, 124.9, 119.7, 117.5, 117.3, 114.7, 114.5, 114.4, 113.2, 104.4, 101.1, 61.7, 57.2, 56.3, 20.5; HRMS-ESI(+): *m/z* 510.2137 $[M+H]^+$, calcd for $C_{29}H_{28}N_5O_4^+$ 510.2136.

*4.18.12.(E)-N'-(2,4-dihydroxybenzylidene)-5-((8-methoxy-2-methylquinolin-4-yl)amino)-1H-indole-2-carbohydrazide (**10l**).* Yellow solid (55.0 mg, 57.2%), mp: 244-246□. ^{1}H NMR (600 MHz, DMSO-d_6): δ 12.01 (br s, 1H), 11.91 (s, 1H), 11.38 (br s, 1H), 8.85 (br s, 1H), 8.53 (s, 1H), 7.92 (d, *J* = 8.3 Hz, 1H), 7.62-7.64 (m, 1H), 7.55 (d, *J* = 8.6 Hz, 1H), 7.34-7.39 (m, 2H), 7.31 (s, 1H), 7.23 (dd, *J* = 2.0, 8.6 Hz, 1H), 7.12 (d, *J* = 7.7 Hz, 1H), 6.54 (s, 1H), 6.4 (dd, *J* = 2.2, 8.4 Hz, 1H), 6.35 (d, *J* = 2.0 Hz, 1H), 3.92 (s, 3H), 2.38 (s, 3H); ^{13}C NMR (151 MHz, DMSO-d_6): δ 161.2, 159.8, 157.5,

157.2, 155.0, 150.5, 148.7, 140.0, 135.2, 133.0, 131.5, 131.2, 128.1, 124.5, 124.1, 123.0, 119.0, 117.9, 113.8, 111.2, 109.0, 108.2, 103.9, 103.1, 101.2, 55.9, 25.3; HRMS-ESI(+): *m/z* 482.1824 $[M+H]^+$, calcd for $C_{27}H_{24}N_5O_4^+$ 482.1823.

*4.1.8.13.(E)-N'-(2,5-dihydroxybenzylidene)-5-((8-methoxy-2-methylquinolin-4-yl)amino)-1H-indole-2-carbohydrazide (**10m**).* Yellow solid (88.0 mg, 91.4%), mp: 238-240□. ^{1}H NMR (600 MHz, DMSO-d_6): δ 12.10 (br s, 1H), 11.97 (br s, 1H), 10.29 (br s, 1H), 9.02 (br s, 1H), 8.61 (s, 1H), 7.98 (d, *J* = 8.4 Hz, 1H), 7.64-7.69 (m, 1H), 7.58 (d, *J* = 8.6 Hz, 1H), 7.43 (t, *J* = 8.2 Hz, 1H), 7.37 (s, 1H), 7.25 (dd, *J* = 1.9, 8.7 Hz, 1H), 7.22 (d, *J* = 7.7 Hz, 1H), 7.05 (s, 1H), 6.77 (d, *J* = 8.8 Hz, 1H), 6.72-6.76 (m, 1H), 6.54 (s, 1H), 3.96 (s, 3H), 2.42 (s, 3H); ^{13}C NMR (151 MHz, DMSO-d_6): δ 162.6, 157.7, 156.7, 152.0, 151.6, 150.6, 150.4, 147.1, 135.5, 131.3, 128.1, 124.8, 123.1, 119.8, 119.4, 118.6, 118.3, 117.7, 117.5, 115.5, 113.9, 113.8, 109.9, 104.2, 101.1, 56.2, 24.3; HRMS-ESI(+): *m/z* 482.1825 $[M+H]^+$, calcd for $C_{27}H_{24}N_5O_4^+$ 482.1823.

*4.1.8.14.(E)-N'-(3,4-dimethoxybenzylidene)-5-((8-methoxy-2-methylquinolin-4-yl)amino)-1H-indole-2-carbohydrazide (**10n**).* Yellow solid (67.0 mg, 65.8%), mp: 246-248□. ^{1}H NMR (600 MHz, DMSO-d_6): δ 12.08 (br s, 1H), 11.93 (s, 1H), 10.66 (br s, 1H), 8.42 (s, 1H), 8.20 (d, *J* = 8.6 Hz, 1H), 7.78 (s, 1H), 7.64-7.72 (m, 2H), 7.56 (d, *J* = 8.1 Hz, 1H), 7.42 (br s, 1H), 7.37 (s, 1H), 7.28 (dd, *J* = 1.7, 8.5 Hz, 1H), 7.24 (d, *J* = 7. 9 Hz, 1H), 7.05 (d, *J* = 8.4 Hz, 1H), 6.56 (s, 1H), 4.11 (s, 3H), 3.85 (s, 3H), 3.83 (s, 3H), 2.58 (s, 3H). ^{13}C NMR (151 MHz, DMSO-d_6): δ 158.2, 157.7, 155.4, 154.8, 151.3, 149.6, 148.2, 136.3, 132.2, 130.3, 129.9, 128.1, 127.4, 127.0, 122.8, 122.4, 119.6, 117.3, 114.5, 114.4, 113.1, 112.0, 108.7, 104.3, 101.0, 57.1, 56.1, 56.0, 20.6. HRMS-ESI(+): *m/z* 510.2134 $[M+H]^+$, calcd for $C_{29}H_{28}N_5O_4^+$ 510.2136.

*4.1.8.15.(E)-N'-(3-bromo-4-methoxybenzylidene)-5-((8-methoxy-2-methylquinolin-4-yl)amino)-1H-indole-2-carbohydrazide (**10o**).* White solid (36.0 mg, 32.3%), mp: 223-225□. ^{1}H NMR (600 MHz, DMSO-d_6): δ 12.10 (br s, 1H), 12.06 (br s, 1H), 10.53 (br s, 1H), 8.40 (s, 1H), 8.18 (d, *J* = 8.4 Hz, 1H), 7.99 (d, *J* = 1.7 Hz, 1H), 7.77

(s, 1H), 7.74 (d, *J* = 8.3 Hz, 1H), 7.62-7.68 (m, 2H), 7.52 (d, *J* = 8.1 Hz, 1H), 7.43 (br s, 1H), 7.25-7.31 (m, 1H), 7.22 (d, *J* = 8.6 Hz, 1H), 6.57 (s, 1H), 4.09 (s, 3H), 3.92 (s, 3H), 2.56 (s, 3H); ^{13}C NMR (151 MHz, DMSO-d_6): δ 158.2, 157.8, 157.2, 155.0, 155.0, 150.0, 146.2, 136.2, 132.0, 131.3, 130.2, 128.8, 128.0, 126.8, 122.9, 119.5, 117.4, 116.9, 114.4, 114.3, 113.3, 112.8, 111.7, 104.4, 101.0, 57.0, 57.0, 20.9; HRMS-ESI(+): *m/z* 558.1135, 560.1117 $[M+H]^+$, calcd for $C_{28}H_{25}BrN_5O_3^+$ 558.1135, 560.1115.

*4.1.8.16.(E)-N'-(2-hydroxy-5-nitrobenzylidene)-5-((8-methoxy-2-methylquinolin-4-yl) amino)-1H-indole-2-carbohydrazide (**10p**).* White solid (51.0 mg, 50%), mp: 222-224□. ^{1}H NMR (600 MHz, DMSO-d_6): δ 12.40 (br s, 1H), 12.18 (br s, 1H), 10.72 (s, 1H), 8.77 (s, 1H), 8.61 (d, *J* = 2.8 Hz, 1H), 8.20 (d, *J* = 8.4 Hz, 1H), 8.18 (dd, *J* = 2.8, 9.1 Hz, 1H), 7.81 (s, 1H), 7.64-7.71 (m, 2H), 7.56 (d, *J* = 8.1 Hz, 1H), 7.47 (br s, 1H), 7.27-7.31 (m, 1H), 7.14 (d, *J* = 9.0 Hz, 1H), 6.57 (s, 1H), 4.11 (s, 3H), 2.58 (s, 3H); ^{13}C NMR (151 MHz, DMSO-d_6): δ 163.0, 157.8, 155.6, 154.7, 149.4, 143.7, 140.4, 136.5, 131.6, 130.0, 129.9, 128.0, 127.1, 127.0, 123.5, 123.1, 120.8, 119.8, 117.5, 117.2, 114.5, 114.4, 113.2, 104.9, 101.0, 57.2, 20.4; HRMS-ESI(+): *m/z* 511.1725 $[M+H]^+$, calcd for $C_{27}H_{23}N_6O_5^+$ 511.1724.

*4.1.8.17.(E)-N'-(2-bromo-5-(trifluoromethyl)benzylidene)-5-((8-methoxy-2-methylquinolin-4-yl)amino)-1H-indole-2-carbohydrazide (**10q**).* Yellow solid (102.0 mg, 85.7%), mp: 222-224□. ^{1}H NMR (600 MHz, DMSO-d_6): δ 12.48 (br s, 1H), 12.19 (br s, 1H), 10.72 (s, 1H), 8.88 (br s, 1H), 8.25 (d, *J* = 2.0 Hz, 1H), 8.21 (d, *J* = 8.6 Hz, 1H), 7.99 (d, *J* = 8.4 Hz, 1H), 7.82 (br s, 1H), 7.75 (dd, *J* = 2.2, 8.4 Hz, 1H), 7.67-7.72 (m, 2H), 7.57 (d, *J* = 8.1 Hz, 1H), 7.49 (br s, 1H), 7.31 (dd, *J* = 1.8, 8.6 Hz, 1H), 6.58 (s, 1H), 4.12 (s, 3H), 2.59 (s, 3H); ^{13}C NMR (151 MHz, DMSO-d_6): δ 158.4, 158.1, 155.6, 154.7, 149.4, 144.6, 135.1, 134.7, 130.0, 130.0, 129.4, 129.2, 128.0, 128.0, 127.2, 125.0, 123.7, 123.2, 123.2, 119.8, 118.8, 117.2, 114.5, 113.2, 105.0, 101.1, 57.2, 20.4; HRMS-ESI(+): *m/z* 596.0904, 598.0884 $[M+H]^+$, calcd for $C_{28}H_{22}BrF_3N_5O_2^+$ 596.0903, 598.0883.

*4.1.8.18.(E)-5-((8-methoxy-2-methylquinolin-4-yl)amino)-N'-(4-methoxy-3-(trifluoro methyl)benzylidene)-1H-indole-2-carbohydrazide (**10r**).* Yellowish solid (32.0 mg, 29.3%), mp: 228-230□. ^{1}H NMR (600 MHz, DMSO-d_6): δ12.03 (br s, 1H), 11.96 (br s, 1H), 8.47 (br s, 1H), 8.01-8.04 (m, 2H), 7.98 (d, *J* = 8.4 Hz, 1H), 7.66 (d, *J* = 1.8 Hz, 1H), 7.58 (d, *J* = 8.6 Hz, 1H), 7.43 (t, *J* = 8.1 Hz, 1H), 7.39 (d, *J* = 9.0 Hz, 1H), 7.37 (br s, 1H), 7.25 (dd, *J* = 1.8, 8.6 Hz, 1H), 7.21 (d, *J* = 7.7 Hz, 1H), 6.55 (s, 1H), 3.97 (s, 3H), 3.96 (s, 3H), 2.42 (s, 3H); ^{13}C NMR (151 MHz, DMSO-d_6): δ161.5, 160.7, 158.6, 156.8, 151.5, 146.1, 135.5, 134.8, 133.6, 132.0, 128.2, 128.0, 127.2, 124.9, 124.8, 124.7, 123.1, 122.2, 118.7, 118.2, 118.0, 117.8, 113.9, 113.9, 113.8, 104.2, 102.4, 101.1, 57.0, 56.2, 24.4; HRMS-ESI(+): *m/z* 548.1904 $[M+H]^+$, calcd for $C_{29}H_{25}F_3N_5O_3^+$ 548.1904.

*4.1.8.19.(E)-N'-(4-fluoro-3-(trifluoromethyl)benzylidene)-5-((8-methoxy-2-methylquin olin-4-yl)amino)-1H-indole-2-carbohydrazide (**10s**).* Yellow solid (28.0 mg, 26.2%), mp: 242-244□. ^{1}H NMR (600 MHz, DMSO-d_6): δ12.29 (br s, 1H), 12.16 (br s, 1H), 10.70 (br s, 1H), 8.56 (br s, 1H), 8.21 (d, *J* = 8.4 Hz, 1H), 8.1 (d, *J* = 6.2 Hz, 2H), 7.80 (s, 1H), 7.61-7.73 (m, 3H), 7.56 (d, *J* = 7.89 Hz, 1H), 7.47 (br. s., 1H), 7.27-7.34 (m, 1H), 6.57 (s, 1H), 4.12 (s, 3H), 2.59 (s, 3H); ^{13}C NMR (151 MHz, DMSO-d_6): δ159.1, 158.0, 155.5, 154.7, 149.5, 145.2, 136.4, 134.2, 132.1, 131.8, 130.1, 129.9, 128.0, 127.1, 125.8, 123.8, 123.0, 122.0, 119.7, 118.6, 118.4, 117.3, 114.5, 114.4, 113.2, 104.8, 101.0, 57.1, 20.5; HRMS-ESI(+): *m/z* 536.1704 $[M+H]^+$, calcd for $C_{28}H_{22}F_4N_5O_2^+$ 536.1704.

*4.1.8.20.(E)-N'-(2,4-bis(trifluoromethyl)benzylidene)-5-((8-methoxy-2-methylquinolin -4-yl)amino)-1H-indole-2-carbohydrazide (**10t**).* Yellow solid (103.0 mg, 88.0%), mp: 231-233□. ^{1}H NMR (600 MHz, DMSO-d_6): δ 12.55 (br s, 1H), 12.24 (br s, 1H), 10.72 (s, 1H), 8.89 (br s, 1H), 8.49 (d, *J* = 8.3 Hz, 1H), 8.16-8.25 (m, 2H), 8.13 (s, 1H), 7.79-7.86 (m, 1H), 7.63-7.73 (m, 2H), 7.57 (d, *J* = 7.9 Hz, 1H), 7.49 (br s, 1H), 7.32 (dd, *J* = 2.0, 8.6 Hz, 1H), 6.59 (s, 1H), 4.12 (s, 3H), 2.58 (s, 3H); ^{13}C NMR (151 MHz, DMSO-d_6): δ 158.4, 158.2, 155.6, 154.7, 149.4, 141.2, 136.8, 136.5, 136.2, 130.2, 130.0, 128.6, 128.0, 127.8, 127.2, 126.5, 124.7, 124.7, 123.6, 123.3, 122.9,

119.8, 118.8, 117.2, 116.8, 114.5, 113.2, 105.2, 101.1, 57.2, 20.4; HRMS-ESI(+): *m/z* 586.1672 $[M+H]^+$, calcd for $C_{29}H_{22}F_6N_5O_2^+$ 586.1672.

*4.1.8.21.(E)-N'-(2,4-dimethoxybenzylidene)-5-((8-methoxy-2-methylquinolin-4-yl)amino)-1H-indole-2-carbohydrazide (**10u**).* Yellowish solid (85.0 mg, 83.5%), mp: 248-250□. ^{1}H NMR (600 MHz, DMSO-d_6): δ 11.92 (br s, 1H), 11.84 (s, 1H), 8.73 (s, 1H), 7.98 (d, *J* = 8.4 Hz, 1H), 7.85 (d, *J* = 9.0 Hz, 1H), 7.62-7.67 (m, 1H), 7.57 (d, *J* = 8.6 Hz, 1H), 7.43 (t, *J* = 8.1 Hz, 1H), 7.36 (br s, 1H), 7.20-7.25 (m, 2H), 6.63-6.69 (m, 2H), 6.54 (s, 1H), 3.96 (s, 3H), 3.88 (s, 3H), 3.84 (s, 3H), 2.42 (s, 3H); ^{13}C NMR (151 MHz, DMSO-d_6): δ 162.9, 159.6, 157.7, 156.7, 156.0, 143.2, 135.4, 132.0, 131.7, 128.2, 128.1, 127.2, 124.7, 122.9, 118.6, 118.2, 115.6, 113.9, 113.9, 107.0, 106.9, 103.8, 101.1, 98.8, 98.7, 56.3, 56.2, 55.9, 15.6; HRMS-ESI(+): *m/z* 510.2134 $[M+H]^+$, calcd for $C_{29}H_{28}N_5O_4^+$ 510.2136.

*4.1.8.22.(E)-N'-(2,6-dimethoxybenzylidene)-5-((8-methoxy-2-methylquinolin-4-yl)amino)-1H-indole-2-carbohydrazide (**10v**).* Yellow solid (47.0 mg,46.2%), mp: 204-206□. ^{1}H NMR (600 MHz, DMSO-d_6): δ 11.70 (br s, 1H), 11.61 (s, 1H), 8.50 (s, 1H), 7.94 (d, *J* = 8.3 Hz, 1H), 7.85 (s, 1H), 7.62-7.67 (m, 1H), 7.60 (d, *J* = 8.6 Hz, 1H), 7.33-7.41 (m, 2H), 7.20-7.28 (m, 1H), 7.15 (d, *J* = 7.7 Hz, 1H), 6.81 (d, *J* = 8.3 Hz, 1H), 6.75 (d, *J* = 8.4 Hz, 1H), 6.53-6.58 (m, 1H), 3.95 (s, 6H), 3.83 (s, 3H), 2.39 (s, 3H); ^{13}C NMR (151 MHz, DMSO-d_6): δ 161.1, 159.2, 157.0, 154.6, 150.8, 139.5, 134.8, 131.9, 131.7, 131.1, 128.1, 124.3, 123.2, 118.9, 118.1, 113.8, 113.8, 110.8, 110.2, 109.3, 105.0, 104.9, 104.8, 101.1, 56.7, 56.0, 25.0; HRMS-ESI(+): *m/z* 510.2134 $[M+H]^+$, calcd for $C_{29}H_{28}N_5O_4^+$ 510.2136.

*4.1.8.23.(E)-N'-(3,5-dimethoxybenzylidene)-5-((8-methoxy-2-methylquinolin-4-yl)amino)-1H-indole-2-carbohydrazide (**10w**).* Yellow solid (92.0 mg, 90.4%), mp: 198-200□. ^{1}H NMR (600 MHz, DMSO-d_6): δ 12.07 (br s, 2H), 8.42 (s, 1H), 8.14 (d, *J* = 8.4 Hz, 1H), 7.75 (s, 1H), 7.64 (d, *J* = 8.6 Hz, 1H), 7.61 (t, *J* = 8.3 Hz, 1H), 7.46 (d, *J* = 8.1 Hz, 1H), 7.43 (s, 1H), 7.28 (dd, *J* = 1.8, 8.6 Hz, 1H), 6.91 (br s, 2H), 6.58-6.61 (m, 1H), 6.56 (s, 1H), 4.07 (s, 3H), 3.82 (s, 6H), 2.53 (s, 3H); ^{13}C NMR

(151 MHz, DMSO-d_6): δ 162.0, 161.2, 161.1, 157.9, 155.3, 147.8, 136.8, 136.1, 131.8, 128.0, 126.4, 122.9, 119.2, 117.7, 114.3, 114.3, 112.2, 106.5, 105.3, 104.5, 104.0, 102.7, 101.1, 56.9, 55.8, 21.6; HRMS-ESI(+): *m/z* 510.2134 $[M+H]^+$, calcd for $C_{29}H_{28}N_5O_4^+$ 510.2136.

*4.1.8.24.(E)-5-((8-methoxy-2-methylquinolin-4-yl)amino)-N'-(2,3,4-trimethoxybenzylidene)-1H-indole-2-carbohydrazide (**10x**).* Yellow solid (102.0 mg, 94.6%), mp: 243-245□. ^{1}H NMR (600 MHz, DMSO-d_6): δ 11.95 (br s, 1H), 11.90 (s, 1H), 8.65 (s, 1H), 8.00 (d, *J* = 8.4 Hz, 1H), 7.64-7.68 (m, 2H), 7.58 (d, *J* = 8.4 Hz, 1H), 7.45 (t, *J* = 8.2 Hz, 1H), 7.36 (s, 1H), 7.22-7.26 (m, 2H), 6.96 (d, *J* = 9.0 Hz, 1H), 6.54 (s, 1H), 3.98 (s, 3H), 3.88 (s, 3H), 3.87 (s, 3H), 3.80 (s, 3H), 2.43 (s, 3H); ^{13}C NMR (151 MHz, DMSO-d_6): δ 157.7, 156.7, 156.5, 155.6, 154.0, 153.1, 143.3, 142.0, 135.5, 131.7, 128.1, 125.0, 122.9, 121.0, 120.9, 120.2, 118.5, 118.3, 114.0, 113.9, 109.2, 109.1, 108.8, 104.0, 101.1, 62.3, 61.0, 56.5, 56.3, 15.6; HRMS-ESI(+): *m/z* 540.2242 $[M+H]^+$, calcd for $C_{30}H_{30}N_5O_5^+$ 540.2241.

*4.1.8.25.(E)-5-((8-methoxy-2-methylquinolin-4-yl)amino)-N'-(3,4,5-trimethoxybenzylidene)-1H-indole-2-carbohydrazide (**10y**).* Yellow solid (91.0 mg, 84.4%), mp: 193-195□. ^{1}H NMR (600 MHz, DMSO-d_6): δ 11.94 (s, 1H), 11.76 (s, 1H), 8.41 (br s, 1H), 7.99 (d, *J* = 8.4 Hz, 1H), 7.65-7.68 (m, 1H), 7.58 (d, *J* = 8.6 Hz, 1H), 7.44 (t, *J* = 8.2 Hz, 1H), 7.37 (br s, 1H), 7.26 (s, 1H), 7.25 (s, 1H), 7.24 (d, *J* = 2.0 Hz, 1H), 7.22 (s, 1H), 7.06 (br s, 1H), 6.54 (s, 1H), 3.98 (s, 3H), 3.87 (s, 6H), 3.73 (s, 3H), 2.42 (s, 3H); ^{13}C NMR (151 MHz, DMSO-d_6): δ 161.7, 161.5, 157.9, 156.6, 153.8, 153.7, 153.6, 143.3, 132.1, 132.0, 130.3, 128.2, 124.8, 122.2, 118.6, 113.9, 113.8, 107.2, 106.0, 104.8, 102.4, 101.1, 101.1, 60.6, 56.5, 56.5, 16.5; HRMS-ESI(+): *m/z* 540.2242 $[M+H]^+$, calcd for $C_{30}H_{30}N_5O_5^+$ 540.2241.

*4.1.8.26.(E)-N'-(3,5-di-tert-butyl-4-hydroxybenzylidene)-5-((8-methoxy-2-methylquinolin-4-yl)amino)-1H-indole-2-carbohydrazide (**10z**).* Yellow solid (101.0 mg, 87.5%). ^{1}H NMR (600 MHz, DMSO-d_6): δ 11.75 (br s, 1H), 9.83 (br s, 1H), 8.42 (s, 1H), 7.97 (dd, *J* = 2.9, 8.1 Hz, 1H), 7.65 (s, 1H), 7.54-7.60 (m, 2H), 7.48-7.54 (m, 2H), 7.41 (t,

J = 8.1 Hz, 1H), 7.14-7.23 (m, 2H), 6.52 (s, 1H), 3.95 (s, 3H), 2.41 (s, 3H), 1.41 (s, 18H); ^{13}C NMR (151 MHz, DMSO-d_6): δ 161.5, 156.8, 156.7, 149.4, 139.8, 139.1, 134.9, 132.5, 132.0, 128.2, 127.3, 125.6, 124.6, 124.4, 122.3, 118.7, 117.9, 113.9, 113.7, 103.8, 102.4, 101.1, 101.1, 56.2, 35.0, 30.6, 30.3; HRMS-ESI(+): *m/z* 578.3124 $[M+H]^+$, calcd for $C_{35}H_{40}N_5O_3^+$ 578.3126.

*4.1.8.27.(E)-N'-((1H-pyrrol-2-yl)methylene)-5-((8-methoxy-2-methylquinolin-4-yl)amino)-1H-indole-2-carbohydrazide (**10A**).* Yellow solid (70.0 mg, 79.9%), mp: 212-214□. ^{1}H NMR (600 MHz, DMSO-d_6): δ 11.76 (s, 1H), 11.66 (s, 1H), 11.57 (br s, 1H), 9.83 (s, 1H), 8.31 (s, 1H), 7.98 (d, *J* = 8.4 Hz, 1H), 7.54-7.58 (m, 1H), 7.53 (d, *J* = 8.6 Hz, 1H), 7.43 (t, *J* = 8.2 Hz, 1H), 7.20-7.25 (m, 2H), 7.18 (dd, *J* = 2.0, 8.6 Hz, 1H), 7.09-7.14 (m, 1H), 6.94 (br s, 1H), 6.47-6.56 (m, 2H), 3.96 (s, 3H), 2.41 (s, 3H); ^{13}C NMR (151 MHz, DMSO-d_6): δ 161.5, 157.5, 156.6, 153.7, 151.7, 135.3, 135.0, 132.0, 128.2, 127.5, 124.8, 123.0, 122.2, 118.6, 118.6, 118.0, 114.0, 113.8, 113.8, 110.0, 103.6, 102.4, 101.1, 56.2, 24.2; HRMS-ESI(+): *m/z* 439.1878 $[M+H]^+$, calcd for $C_{25}H_{23}N_6O_2^+$ 439.1877.

*4.1.8.28.(E)-5-((8-methoxy-2-methylquinolin-4-yl)amino)-N'-(thiophen-2-ylmethylene)-1H-indole-2-carbohydrazide (**10B**).* Yellow solid (80.0 mg, 87.9%), mp: 207-209□. ^{1}H NMR (600 MHz, DMSO-d_6): δ 12.11 (br s, 1H), 12.02 (s, 1H), 10.72 (s, 1H), 8.70 (s, 1H), 8.19 - 8.23 (m, 1H), 7.79 (s, 1H), 7.67 - 7.72 (m, 2H), 7.66 (d, *J* = 8.4 Hz, 1H), 7.57 (d, *J* = 8.1 Hz, 1H), 7.51 (d, *J* = 2.9 Hz, 1H), 7.41 (br s, 1H), 7.28 (dd, *J* = 1.7, 8.6 Hz, 1H), 7.17 (dd, *J* = 3.7, 5.0 Hz, 1H), 6.57 (s, 1H), 4.12 (s, 3H), 2.58 (s, 3H). ^{13}C NMR (151 MHz, DMSO-d_6): δ 158.4, 158.2, 155.6, 154.7, 149.4, 143.1, 139.5, 136.3, 131.5, 130.0, 129.8, 129.5, 128.4, 128.0, 127.2, 122.8, 119.7, 117.2, 114.5, 114.4, 113.3, 104.4, 101.0, 57.2, 20.4. HRMS-ESI(+): *m/z* 456.1487 $[M+H]^+$, calcd for $C_{25}H_{22}N_5O_2S^+$ 456.1489.

*4.1.8.29.(E)-5-((8-methoxy-2-methylquinolin-4-yl)amino)-N'-(pyridin-2-ylmethylene)-1H-indole-2-carbohydrazide (**10C**).* Yellow solid (47.0 mg, 52.2%), mp: 195-197□. ^{1}H NMR (600 MHz, DMSO-d_6): δ 12.27 (br s, 1H), 11.97 (s, 1H), 10.74 (s, 1H),

8.63-8.66 (m, 1H), 8.21 (t, *J* = 8.3 Hz, 2H), 7.89-7.94 (m, 1H), 7.83 (br s, 1H), 7.69-7.71 (m, 2H), 7.62 (d, *J* = 8.6 Hz, 1H), 7.58 (d, *J* = 4.8 Hz, 1H), 7.43-7.46 (m, 1H), 7.23 (dd, *J* = 1.7, 8.6 Hz, 1H), 7.19 - 7.21 (m, 1H), 6.58 (s, 1H), 4.12 (s, 3H), 2.59 (s, 3H); ^{13}C NMR (151 MHz, DMSO-d_6): δ 161.2, 158.5, 158.2, 155.6, 154.7, 154.7, 149.4, 135.9, 132.2, 130.0, 129.6, 128.1, 127.2, 127.1, 122.2, 119.4, 117.2, 117.2, 114.5, 114.4, 114.3, 113.2, 103.1, 101.0, 57.2, 20.4; HRMS-ESI(+): *m/z* 451.1876 $[M+H]^+$, calcd for $C_{26}H_{23}N_6O_2^+$ 451.1877.

*4.1.8.30.(E)-5-((8-methoxy-2-methylquinolin-4-yl)amino)-N'-(pyridin-3-ylmethylene)-1H-indole-2-carbohydrazide (**10D**).* Yellow solid (58.0 mg, 64.4%), mp: 220-222□. ^{1}H NMR (600 MHz, DMSO-d_6): δ 12.21 (br s, 1H), 12.15 (br s, 1H), 10.69 (br s, 1H), 8.90 (br s, 1H), 8.64 (dd, *J* = 1.6, 4.7 Hz, 1H), 8.54 (br s, 1H), 8.15-8.23 (m, 2H), 7.80 (br s, 1H), 7.68-7.73 (m, 1H), 7.66 (d, *J* = 8.6 Hz, 1H), 7.57 (d, *J* = 8.1 Hz, 1H), 7.52 (dd, *J* = 4.8, 7.7 Hz, 1H), 7.46 (br s, 1H), 7.28 (dd, *J* = 2.0, 8.6 Hz, 1H), 6.57 (s, 1H), 4.12 (s, 3H), 2.58 (s, 3H); ^{13}C NMR (151 MHz, DMSO-d_6): δ 158.2, 157.9, 155.6, 154.8, 151.2, 149.4, 149.2, 145.1, 133.9, 130.7, 130.1, 128.0, 127.1, 124.5, 123.0, 119.8, 118.9, 117.2, 116.9, 114.5, 114.4, 113.2, 104.7, 101.1, 57.2, 20.5; HRMS-ESI(+): *m/z* 451.1876 $[M+H]^+$, calcd for $C_{26}H_{23}N_6O_2^+$ 451.1877.

*4.1.8.31.(E)-5-((8-methoxy-2-methylquinolin-4-yl)amino)-N'-(pyridin-4-ylmethylene)-1H-indole-2-carbohydrazide (**10E**).* Yellow solid (68.0 mg, 75.6%), mp: 222-224□. ^{1}H NMR (600 MHz, DMSO-d_6): δ 12.37 (br s, 1H), 12.19 (br s, 1H), 10.70 (s, 1H), 8.73 (d, *J* = 5.9 Hz, 2H), 8.49 (br s, 1H), 8.21 (d, *J* = 8.4 Hz, 1H), 7.82 (d, *J* = 6.05 Hz, 3H), 7.68-7.74 (m, 1H), 7.66 (d, *J* = 8.6 Hz, 1H), 7.58 (d, *J* = 7.9 Hz, 1H), 7.48 (br s, 1H), 7.30 (dd, *J* = 1.9, 8.7 Hz, 1H), 6.57 (s, 1H), 4.12 (s, 3H), 2.58 (s, 3H); ^{13}C NMR (151 MHz, DMSO-d_6): δ 161.3, 158.5, 158.3, 158.1, 155.6, 154.7, 149.4, 130.0, 129.5, 128.0, 127.2, 123.2, 122.2, 122.0, 119.9, 118.1, 117.2, 116.2, 114.5, 113.3, 103.5, 101.1, 57.2, 20.4; HRMS-ESI(+): *m/z* 451.1875 $[M+H]^+$, calcd for $C_{26}H_{23}N_6O_2^+$ 451.1877.

4.1.8.32.(E)-5-((8-methoxy-2-methylquinolin-4-yl)amino)-N'-((4-methoxynaphthalen-

*1-yl)methylene)-1H-indole-2-carbohydrazide (**10F**).* Yellowish solid (85.0 mg, 80.3%), mp: 218-220□. ^{1}H NMR (600 MHz, DMSO-d_6): δ 11.98 (br s, 1H), 11.91 (s, 1H), 9.00 (s, 1H), 8.96 (d, *J* = 8.6 Hz, 1H), 8.28 (d, *J* = 7. 9 Hz, 1H), 8.02 (d, *J* = 8.4 Hz, 1H), 7.91 (d, *J* = 8.1 Hz, 1H), 7.72-7.75 (m, 1H), 7.69-7.71 (m, 1H), 7.59-7.64 (m, 2H), 7.49 (t, *J* = 8.1 Hz, 1H), 7.39 (br s, 1H), 7.29 (d, *J* = 7.5 Hz, 1H), 7.26 (dd, *J* = 1.8, 8.6 Hz, 1H), 7.12-7.14 (m, 1H), 6.56 (s, 1H), 4.06 (s, 3H), 3.99 (s, 3H), 2.45 (s, 3H); ^{13}C NMR (151 MHz, DMSO-d_6): δ 162.4, 158.0, 157.8, 157.1, 148.2, 133.3, 132.1, 131.8, 131.6, 130.1, 128.5, 128.4, 128.1, 126.4, 126.3, 126.0, 125.5, 125.5, 124.9, 122.9, 122.6, 122.5, 122.4, 122.3, 118.4, 114.0, 104.9, 104.0, 101.1, 56.5, 56.4, 19.0; HRMS-ESI(+): *m/z* 530.2187 $[M+H]^+$, calcd for $C_{32}H_{28}N_5O_3^+$ 530.2187.

*4.1.8.33.(E)-5-((8-methoxy-2-methylquinolin-4-yl)amino)-N'-(quinolin-4-ylmethylene) -1H-indole-2-carbohydrazide (**10G**).* Yellow solid (50.0 mg, 50.0%), mp: 222-224□. ^{1}H NMR (600 MHz, DMSO-d_6): δ 12.47 (br s, 1H), 12.21 (br s, 1H), 10.56 (br s, 1H), 9.18 (br s, 1H), 9.02 (d, *J* = 4.4 Hz, 1H), 8.72-8.80 (m, 1H), 8.19 (d, *J* = 8.4 Hz, 1H), 8.13 (d, *J* = 8.4 Hz, 1H), 7.91 (br s, 1H), 7.84-7.89 (m, 1H), 7.81-7.83 (m, 1H), 7.77 (t, *J* = 7.4 Hz, 1H), 7.64-7.72 (m, 2H), 7.52 (d, *J* = 8.1 Hz, 2H), 7.32 (dd, *J* = 1.8, 8.6 Hz, 1H), 6.58 (s, 1H), 4.10 (s, 3H), 2.57 (s, 3H); ^{13}C NMR (151 MHz, DMSO-d_6): δ 158.5, 158.3, 158.1, 155.1, 155.0, 150.9, 149.9, 148.9, 144.8, 137.8, 131.7, 131.0, 130.3, 130.2, 128.1, 126.8, 125.2, 124.6, 123.2, 120.1, 119.7, 118.8, 117.4, 116.8, 114.4, 112.8, 105.0, 101.1, 57.0, 20.9; HRMS-ESI(+): *m/z* 501.2035 $[M+H]^+$, calcd for $C_{30}H_{25}N_6O_2^+$ 501.2034.

*4.1.8.34.(E)-N'-((2-chloroquinolin-3-yl)methylene)-5-((8-methoxy-2-methylquinolin-4 -yl)amino)-1H-indole-2-carbohydrazide (**10H**).* Yellow solid (71.0 mg, 66.5%), mp: 254-256□. ^{1}H NMR (600 MHz, DMSO-d_6): δ 12.42 (br s, 1H), 12.10 (br s, 1H), 9.01 (s, 1H), 8.96 (br s, 1H), 8.27 (d, *J* = 7.7 Hz, 1H), 8.05 (d, *J* = 8.4 Hz, 1H), 7.98-8.01 (m, 1H), 7.88 (dt, *J* = 1.4, 7.7 Hz, 1H), 7.69-7.76 (m, 2H), 7.62 (d, *J* = 8.4 Hz, 1H), 7.50 (t, *J* = 8.2 Hz, 1H), 7.44-7.48 (m, 1H), 7.31 (d, *J* = 7.7 Hz, 1H), 7.28 (dd, *J* = 2.0, 8.6 Hz, 1H), 6.56 (s, 1H), 4.01 (s, 3H), 2.47 (s, 3H); ^{13}C NMR (151 MHz, DMSO-d_6): δ 158.0, 156.2, 154.0, 150.6, 149.0, 147.6, 142.7, 139.5, 137.0, 136.2, 135.8, 133.5,

132.3, 131.3, 129.5, 128.4, 128.1, 128.0, 127.4, 126.6, 125.4, 123.8, 123.3, 118.7, 118.3, 114.1, 104.8, 101.1, 56.5, 23.3; HRMS-ESI(+): *m/z* 535.1643, 536.1676 $[M+H]^+$, calcd for $C_{30}H_{24}ClN_6O_2^+$ 535.1644, 536.1678.

*4.1.8.35.(E)-N'-((5-methoxy-2-methyl-1H-indol-3-yl)methylene)-5-((8-methoxy-2-methylquinolin-4-yl)amino)-1H-indole-2-carbohydrazide(**10I**).* Yellowish solid (22.0 mg, 20.7%). ^{1}H NMR (600 MHz, DMSO-d_6): δ 12.10 (s, 1H), 11.81 (s, 1H), 11.45 (s, 1H), 10.82 (s, 1H), 8.79 (s, 1H), 8.29 (d, *J* = 8.6 Hz, 1H), 7.85 (d, *J* = 2.4 Hz, 1H), 7.73-7.79 (m, 1H), 7.64-7.71 (m, 2H), 7.56 (d, *J* = 8.1 Hz, 1H), 7.44 (s, 1H), 7.21-7.28 (m, 2H), 6.78 (dd, *J* = 2.5, 8.7 Hz, 1H), 6.56 (s, 1H), 4.11 (s, 3H), 3.79-3.83 (m, 3H), 2.57-2.60 (m, 3H), 2.52 (s, 3H); ^{13}C NMR (151 MHz, DMSO-d_6): δ 157.0, 155.6, 154.8, 154.6, 149.3, 144.7, 141.0, 136.1, 133.0, 131.2, 130.0, 129.7, 128.2, 127.1, 126.6, 122.4, 119.5, 117.3, 114.7, 114.2, 113.2, 111.8, 111.1, 108.0, 104.7, 103.6, 101.0, 57.2, 55.7, 20.4, 12.0; HRMS-ESI(+): *m/z* 533.2296 $[M+H]^+$, calcd for $C_{31}H_{29}N_6O_3^+$ 533.2296.

4.2. Biological evaluation

4.2.1. Cell culture

The following cell lines are used in our study. HepG2 (HB-8065) and HEK293T (CRL-11268) were purchased from ATCC, while SMMC-7721, LO2, and QGY-7703 from Institute of Biochemistry and Cell Biology (SIBS, CAS). HepG2, SMMC-7721 and HEK293T cells were cultured in Dulbecco's Eagle's medium (DMEM), while LO2, and QGY-7703 cells were cultured in RPIM 1640 medium containing 10% fetal bovine serum (FBS) at 37□ in a humidified atmosphere of 5% CO2 and 95% air.

4.2.2. shRNA transfection

The shNur77 (5`- CCG GTG GTG AAG GAA GTT GTC CGA ACT CGA GTT CGG ACA ACT TCC TTC ACC ATT TTT-3`) transfection was performed using TurboFect (Yeasen, China) transfection reagent according to the manufacturer's instructions. As a negative control, a non-specific scrambled control (scr) was

used[67].

4.2.3. Antibodies

Antibodies includes: anti-Nur77 (D63C5, #3960), anti-Cleaved Caspase-3(Asp175, #9661), anti-p62 (E7M1A, #16177), anti-LC3 (D11, #3868) and anti-Tubulin (D20G3,#5335) from Cell Signaling Technology; anti-Bip, anti-CHOP (15204-1-AP), anti-TRB3 (13300-1-AP), anti-Beclin1 (11306-1-AP), anti-PDI (11245-1-AP), anti-PARP(13371-1-AP) and anti-PCNA (10205-2-AP) from Proteintech.

4.2.4. Cytotoxicity in vitro

The cytotoxicity of all complexes against the three HCC cell lines and a normal cancer cell line, LO2, were detected by the 3-(4,5-dimethylthiazol-2-yl)-2,5-diphenyltetrazolium (MTT) (Sigma, USA) assay according to reported procedures. The cells were incubated with compounds for 48 h at six different concentrations. The concentration range of each complex was selected based on the cytotoxicity. The growth-inhibitory rates of the complexes were calculated as $(OD_{control} - OD_{test})/OD_{control} \times 100\%$. IC_{50} values were calculated using the percentage of growth versus untreated control.

4.2.5. Colony formation assay

Cells (500 units) were counted and seeded in 6-wells plates for colony formation assay. Cells were cultured for 24 h at 37□ and then the media were replaced with media added compound **10g** at the indicated concentrations. After 24 h treatment, the media were changed to normal and cells were cultured for 15 days. The colonies were fixed with 4% paraformaldehyde for 30 min and stained with 0.1% Crystal Violet for 15 min and washed. The colonies were then photographed.

4.2.6. Western Blotting

After treatment, cell lysates were prepared with RIPA buffer in the presence of protease inhibitor cocktails and phosphatase inhibitor cocktails for 30 min on ice.

After centrifugation (12,000 g for 5 min at 4□), the protein supernatants were collected, quantified by the BCA method and total protein content (40-80 μg) was separated by SDS-PAGE and transferred onto 0.45 mm nitrocellulose membranes. Membranes were blocked with 5% non-fat dry milk for 1 h and incubated overnight with primary antibodies and incubated with horseradish peroxidase-linked secondary antibodies. Bands were detected by chemiluminescence imaging system (Bio-Rad, USA).

4.2.7. Nuclear and cytoplasmic protein extraction

After treatment, cells were resuspended in buffer A (10 mM HEPES, 10 mM NaCl, 5 mM EDTA, 1 mM $CaCl_2$, 0.5 mM $MgCl_2$) for 10 min on Ice. Then 0.1% NP40 were added in the lysates and vortex it 10 s. The first round of centrifugation was performed at 15000 rpm for 3 min in a centrifuge at 4□. The cytoplasmic fraction was in the supernatant. The pellets were resuspended and harvest in RIPA for 30 min on ice. Then the Homogenization was performed at 15000 rpm for 15 min in a centrifuge at 4□. The resulting supernatant were nuclear protein. Usually, the concentration of cytoplasmic protein was much higher than that of nuclear proteins when the two were lysed out of the cell. Western blotting detection was performed after adjusting the protein concentration of the two.

4.2.8. Annexin V-FITC/PI binding assay

Cells were plated on six-well plates with a density of 1×10^6 per well. After 24 hours, the cells treated with different concentration of **10g** for 12 hours, and then the suspended and the adherent cells were collected, stained with Annexin V-FITC for 15 min and with propidium iodide for 15 min, and analyzed immediately by flow cytometry system (Attune™ NxT, Thermo, USA).

4.2.9. Mitochondrial membrane potential assay

Cells were plated on six-well plates with a density of 1×10^6 per well. The cells treated with 2 μM **10g** for 12 hours， and then were collected and resuspended in fresh medium. After the addition of 0.5 mL JC-1 working solution, the cells were incubated

at 37□ for 20 min. After washing with the JC-1 staining buffer twice，cells were collected for flow cytometry (Attune™ NxT, Thermo, USA).

4.2.10. Inhibition of autophagy and ER stress

HepG2 cells grown to confluence in 12-well plates were pretreated with 2 mM autophagy inhibitor 3-Methyladenine(3-MA) (Apexbio, USA) or 2 mM ER stress inhibitor Benzenebutyric acid (4-PBA) (Apexbio, USA) for 2 hours. **10g** was then added to the culture medium at the corresponding concentrations for 12 hours.

4.2.11. Immunofluorescent assay by confocal microscopy

Cells were fixed with 4% (v/v) paraformaldehyde for 20 min at room temperature and permeabilized with 0.1% Triton X-100 for 20 min, followed by blocking for 30 min at room temperature with 5% BSA. Cells were then incubated for 1 h with anti-Nur77 antibody (1:500 dilution; Cell Signaling Technology). After washing for three times with PBS, the cells were further incubated for another 1 h with secondary antibodies FITC or Cy3-conjugated anti-rabbit IgG. Subsequently, the cells were washed three times with PBS. All images were collected with a confocal microscope.

4.2.12. In vivo tumor model

We established mice hepatoma homograft model in 4-week-old male Balb/c mice by subcutaneously injecting HepG2 cells (5×10^6) into the flanks of the mice. When each tumor grew to about 100 mm^3, 15 mice were divided randomly into three groups, a vehicle control group, a low dose drug treatment group (10 mg/kg body weight) and a high dose drug treatment group (20 mg/kg body weight). **10g** was administered once every day for 15 days. Then mice were euthanized, and tumors were separated, weighed, and subjected to further analysis. All procedures were performed in compliance with the guidelines from the Institutional Animal Care and Use Committee at the Experimental Animal Centre in Xiamen University.

4.2.13. Hematoxylin and Eosin (H&E) and immunohistochemistry staining

Tumor tissues were fixed in 4% paraformaldehyde and embedded in paraffin. Then, 5 μm thick slices were stained with hematoxylin and eosin and examined by light microscopy. For immunostaining, tumor sections were incubated with anti-Nur77 (1:200 dilution), anti-PCNA (1:100 dilution), anti-LC3 (1:150 dilution), anti-Beclin1 (1:200 dilution), anti-CHOP (1:100 dilution), anti-Bip (1:150 dilution) or anti-TRB3 (1:150 dilution) antibody. The protocols were approved by the Institutional Animal Care and Use Committee of the University of Xiamen University.

4.2.14. Fluorescence quench titration

Nur77-LBD protein solutions were prepared (1 μM protein with and without 4 μM compound) and were mixed in a microplate to obtain 20 different compound concentrations ranging from 0 to 4 μM in approximately 0.2 μM steps. After 30 min incubation at room temperature, fluorescence was measured at 25□ on a Tecan Safire^2 with λ_{ex} = 280 nm and λ_{em} = 340 nm. The setting for slit widths depended on the protein concentration used[68]. Binding curves were analyzed according to the two-state model describing the formation of a 1:1 complex[68].

4.2.15. Surface plasmon resonance (SPR)

The protocols were approved by the Instrumental Analysis and Testing Center, School of Pharmacy, Xiamen University. The binding kinetics between Nur77-LBD and compounds were performed on a BIAcore T200 instrument (GE Healthcare) as described[69].

4.2.16. Statistical analysis

Data were represented as mean ± standard deviation (SD) or median ± SEM. The statistical significance of differences was determined using an analysis of variance or Student *t*-test. A P value of <0.05 was considered as significant. All data were acquired in at least three independent experiments.

4.3. Docking study

Molecular docking was carried out using Glide (Schrödinger 2018-4)[70], a

grid-based docking program was used for the docking study of **10g** to the protein. The crystal structure of Nur77-LBD in complex with **3mj** (PDB ID: 4RE8, retrieved from: https://www.rcsb.org/structure/4RE8) was used. Docking was performed with the implemented standard routine in Glide. Compounds were first docked to protein using Glide SP to predict the potential binding poses. For the top 5 complex conformations were further redocked using Induced Fit docking[71, 72] to explore the best binding model, and the MM/GBSA[73] (Prime MMGBSA v3.000) was used to calculate the absolute binding free energy. Schrödinger's Maestro was used as the primary graphical user interfaces for the visualization of the crystal structure and docking results. The docking results presented here were analyzed by using PyMOL[74], version 2.3.0 (Open-Source PyMOL^{TM} by Schrödinger), such as the poses to check for their binding site surface and interactions with the protein in the docking site.

Notes

The authors declare no competing financial interest.

Acknowledgments

The authors thank Junjie Chen and Cuiling Sun for kindly performing the data analysis on surface plasmon resonance assay and NMR spectroscopy, respectively. They are from the Analysis and Measurement Center, School of Pharmaceutical Sciences, Xiamen University.

This work was supported by the National Natural Science Foundation of China (No. 81773600), the Natural Science Foundation of Fujian Province of China (No. 2018J01132), and the Fundamental Research Funds for the Central Universities (No. 20720180051).

Appendix A. Supplementary data

Supplementary data to this article can be found online at ……

Reference

[1]. H.B. El–Serag, K.L. Rudolph, Hepatocellular carcinoma: epidemiology and molecular carcinogenesis, Gastroenterology, 132 (2007) 2557-2576.

[2]. J. Llovet, A. Burroughs, J. Bruix, Hepatocellular carcinoma [J1, Lancet, 362 (2003) l907-l907.

[3]. J.M. Llovet, R. Montal, D. Sia, R.S. Finn, Molecular therapies and precision medicine for hepatocellular carcinoma, Nature Reviews Clinical Oncology, 15 (2018) 599-616.

[4]. X. Bian, H. Chen, P. Yang, Y. Li, F. Zhang, J. Zhang, W. Wang, W. Zhao, Z. Sheng, Q. Chen, Nur77 suppresses hepatocellular carcinoma via switching glucose metabolism toward gluconeogenesis through attenuating phosphoenolpyruvate carboxykinase sumoylation, Nature Communications, 8 (2017) 14420.

[5]. H. Yang, Y. Nie, Y. Li, Y.-J.Y. Wan, ERK1/2 deactivation enhances cytoplasmic Nur77 expression level and improves the apoptotic effect of fenretinide in human liver cancer cells, Biochemical pharmacology, 81 (2011) 910-916.

[6]. L.C. Chao, K. Wroblewski, Z. Zhang, L. Pei, L. Vergnes, O.R. Ilkayeva, S.Y. Ding, K. Reue, M.J. Watt, C.B. Newgard, Insulin resistance and altered systemic glucose metabolism in mice lacking Nur77, Diabetes, 58 (2009) 2788-2796.

[7]. T.W.H. Pols, R. Ottenhoff, M. Vos, J.H.M. Levels, P.H.A. Quax, J.C.M. Meijers, H. Pannekoek, A.K. Groen, C.J.M.D. Vries, Nur77 modulates hepatic lipid metabolism through suppression of SREBP1c activity, Biochemical & Biophysical Research Communications, 366 (2008) 910-916.

[8]. R.N. Hanna, L.M. Carlin, H.G. Hubbeling, D. Nackiewicz, A.M. Green, J.A. Punt, F. Geissmann, C.C. Hedrick, The transcription factor NR4A1 (Nur77) controls bone marrow differentiation and the survival of Ly6C- monocytes, Nature Immunology, 12 (2011) 778.

[9]. B. Liang, X. Song, G. Liu, R. Li, J. Xie, L. Xiao, M. Du, Q. Zhang, X. Xu, X. Gan, Involvement of TR3/Nur77 translocation to the endoplasmic reticulum in ER stress-induced apoptosis, Experimental cell research, 313 (2007) 2833-2844.

[10]. L. B, K. SK, L. F, L. W, H. YH, C. X, D. MI, R. JC, Z. XK, Conversion of Bcl-2 from protector to killer by interaction with nuclear orphan receptor Nur77/TR3, Cell, 116 (2004) 527-540.

[11]. W. Wang, Y. Wang, H. Chen, Y. Xing, F. Li, Q. Zhang, B. Zhou, H. Zhang, J. Zhang, X. Bian, Orphan nuclear receptor TR3 acts in autophagic cell death via mitochondrial signaling, Nature Chemical Biology, 10 (2014) 133-140.

[12]. Y. Li, B. Lin, A. Agadir, R. Liu, M.I. Dawson, J.C. Reed, J.A. Fontana, F. Bost, P.D. Hobbs, Y. Zheng. Molecular determinants of AHPN (CD437)-induced growth arrest and apoptosis in human lung cancer cell lines, Molecular & Cellular Biology, 18 (1998) 4719.

[13]. A.J. Wilson, D. Arango, J.M. Mariadason, B.G. Heerdt, L.H. Augenlicht, TR3/Nur77 in Colon Cancer Cell Apoptosis, Cancer Research, 63 (2003) 5401.

[14]. M. Sakaue, H. Adachi, M. Dawson, A.M. Jetten, Induction of Egr-1 expression by the retinoid AHPN in human lung carcinoma cells is dependent on activated ERK1/2, Cell Death & Differentiation, 8 (2001) 411-424.

[15]. Y. Pekarsky, C. Hallas, C.M. Croce, Molecular basis of mature T-cell leukemia, Jama, 286 (2001)

2308-2314.
[16]. X. Zhang, Vitamin A and apoptosis in prostate cancer, Endocrine-related cancer, 9 (2002) 87.
[17]. W. Debbie, Autophagy: a new link in the chain, Nature Reviews Molecular Cell Biology, 11 (2010) 604-605.
[18]. F. Janku, D.J. McConkey, D.S. Hong, R. Kurzrock, Autophagy as a target for anticancer therapy, Nature reviews Clinical oncology, 8 (2011) 528.
[19]. J.R. Cubillos-Ruiz, S.E. Bettigole, L.H. Glimcher, Tumorigenic and immunosuppressive effects of endoplasmic reticulum stress in cancer, Cell, 168 (2017) 692-706.
[20]. S. Giuliano, Y. Cormerais, M. Dufies, R. Grépin, P. Colosetti, A. Belaid, J. Parola, A. Martin, S. Lacas-Gervais, N.M. Mazure, Resistance to sunitinib in renal clear cell carcinoma results from sequestration in lysosomes and inhibition of the autophagic flux, Autophagy, 11 (2015) 1891-1904.
[21]. E.H. Baehrecke, Autophagy: dual roles in life and death?, Nature Reviews Molecular Cell Biology, 6 (2005) 505-510.
[22]. L. Beth, Y. Junying, Autophagy in cell death: an innocent convict?, Journal of Clinical Investigation, 115 (2005) 2679-2688.
[23]. M. Hu, Q. Luo, G. Alitongbieke, S. Chong, C. Xu, L. Xie, X. Chen, D. Zhang, Y. Zhou, Z. Wang, X. Ye, L. Cai, F. Zhang, H. Chen, F. Jiang, H. Fang, S. Yang, J. Liu, M.T. Diaz-Meco, Y. Su, H. Zhou, J. Moscat, X. Lin, X.K. Zhang, Celastrol-Induced Nur77 Interaction with TRAF2 Alleviates Inflammation by Promoting Mitochondrial Ubiquitination and Autophagy, Molecular cell, 66 (2017) 141-153.
[24]. R. Sano, J.C. Reed, ER stress-induced cell death mechanisms Biochimica et Biophysica Acta (BBA) - Molecular Cell Research, 1833 (2013) 3460-3470.
[25]. N.J. Darling, S.J. Cook, The role of MAPK signalling pathways in the response to endoplasmic reticulum stress, Biochim Biophys Acta, 1843 (2014) 2150-2163.
[26]. L.C. Chao, Z. Zidong, P. Liming, S. Tsugumichi, T. Peter, P.F. Pilch, Nur77 coordinately regulates expression of genes linked to glucose metabolism in skeletal muscle, Molecular Endocrinology, 21 (2007) 2152-2163.
[27]. L. Pei, A. Castrillo, P. Tontonoz, Regulation of macrophage inflammatory gene expression by the orphan nuclear receptor Nur77, Molecular Endocrinology, 20 (2006) 786-794.
[28]. L.M. Yao, J.P. He, H.Z. Chen, Y. Wang, W.J. Wang, R. Wu, C.D. Yu, Q. Wu, Orphan receptor TR3 participates in cisplatin-induced apoptosis via Chk2 phosphorylation to repress intestinal tumorigenesis, Carcinogenesis, 33 (2012) 301-311.
[29]. Z. Yanyan, D. Xiping, C. Hangzi, L. Jingjing, Z. Bixing, H. Danhong, L. Guideng, X. Qingyan, Z. Mingqing, B.C. Weimer, Cytosporone B is an agonist for nuclear orphan receptor Nur77, Nature Chemical Biology, 4 (2008) 548-556.
[30]. L. Jing-Jing, Z. Hui-Ni, Z. Lian-Ru, Z. Yan-Yan, C. Yan, W. Yuan, W. Juan, X. Shao-Hua, L. Wen-Jun, W. Wei-Jia, A unique pharmacophore for activation of the nuclear orphan receptor Nur77 in vivo and in vitro, Cancer Research, 70 (2010) 3628-3637.
[31]. Y. Hui, N. Bushue, P. Bu, Y.J.Y. Wan, Induction and intracellular localization of Nur77 dictate fenretinide-induced apoptosis of human liver cancer cells, Biochemical Pharmacology, 79 (2010) 948-954.
[32]. Y. Chen, P. Lin, The induction of orphan nuclear receptor Nur77 expression by n-butylenephthalide aspharmaceuticals on hepatocellular carcinoma (HCC) cells therapy, European

Journal of Cancer Supplements, 6 (2008) 141-141.

[33]. L. Po-Cheng, C. Yi-Lin, C. Shao-Chih, Y. Yung-Luen, C. Shee-Ping, C. Min-Hui, C. Kuan-Yen, C. Wen-Liang, L. Shinn-Zong, C. Tzyy-Wen, Orphan nuclear receptor, Nurr-77 was a possible target gene of butylidenephthalide chemotherapy on glioblastoma multiform brain tumor, Journal of Neurochemistry, 106 (2010) 1017-1026.

[34]. C. Li-Fu, L. Po-Cheng, H. Li-Ing, L. Po-Yen, W. Wan-Chen, C. I-Ping, C. Hui-Wen, L. Shinn-Zong, H. Yeu-Chern, H. Horng-Jyh, Overexpression of the orphan receptor Nur77 and its translocation induced by PCH4 may inhibit malignant glioma cell growth and induce cell apoptosis, Journal of Surgical Oncology, 103 (2011) 442-450.

[35]. S. Chintharlapalli, R. Burghardt, S. Papineni, S. Ramaiah, K. Yoon, S. Safe, Activation of Nur77 by selected 1,1-Bis(3'-indolyl)-1-(p-substituted phenyl)methanes induces apoptosis through nuclear pathways, Journal of Biological Chemistry, 280 (2005) 24903-24914.

[36]. K. Siva Kumar, Z. Xiuwen, Z. Xin, L. Bingzhen, C. Ya, S. Kai, T. Xuefei, T. James, C. Xihua, L. Feng, A short Nur77-derived peptide converts Bcl-2 from a protector to a killer, Cancer Cell, 14 (2008) 285-298.

[37]. C. Ferlini, L. Cicchillitti, G. Raspaglio, S. Bartollino, S. Cimitan, C. Bertucci, S. Mozzetti, D. Gallo, M. Persico, C. Fattorusso, G. Campiani, G. Scambia, Paclitaxel Directly Binds to Bcl-2 and Functionally Mimics Activity of Nur77, Cancer Research, 69 (2009) 6906-6914.

[38]. J. Chen, W. Fiskus, K. Eaton, P. Fernandez, Y. Wang, R. Rao, P. Lee, R. Joshi, Y. Yang, R. Kolhe, Cotreatment with BCL-2 antagonist sensitizes cutaneous T-cell lymphoma to lethal action of HDAC7-Nur77–based mechanism, Blood, 113 (2009) 4038-4048.

[39]. L. Wu, L. Chen, Characteristics of Nur77 and its ligands as potential anticancer compounds (Review), Molecular Medicine Reports, 18 (2018) 4793-4801.

[40]. Q. Wu, S. Liu, X.F. Ye, Z.W. Huang, W.J. Su, Dual roles of Nur77 in selective regulation of apoptosis and cell cycle by TPA and ATRA in gastric cancer cells, Carcinogenesis, 23 (2002) 1583-1592.

[41]. R.S. Keri, S.A. Patil, Quinoline: A promising antitubercular target, Biomedicine & Pharmacotherapy, 68 (2014) 1161-1175.

[42]. H. Guo, Isatin derivatives and their anti-bacterial activities, European journal of medicinal chemistry, 164 (2019) 678-688.

[43]. S. Jain, V. Chandra, P.K. Jain, K. Pathak, D. Pathak, A. Vaidya, Comprehensive Review on Current Developments of Quinoline-Based Anticancer Agents, Arabian Journal of Chemistry, 12 (2019) 4920-4946.

[44]. N.A. Koorbanally, S.A. Shintre, K. Gopaul, A Review on the Synthesis and Anti-cancer Activity of 2-substituted Quinolines, Anti-Cancer Agents in Medicinal Chemistry, 15 (2015) 631-646.

[45]. Y. Wan, Y. Li, C. Yan, M. Yan, Z. Tang, Indole: A privileged scaffold for the design of anti-cancer agents, European journal of medicinal chemistry, 183 (2019) 111691.

[46]. L.J. Guo, C.-X. Wei, J.-H. Jia, L.-M. Zhao, Z.-S. Quan, Design and synthesis of 5-alkoxy-[1,2,4]triazolo[4,3-a]quinoline derivatives with anticonvulsant activity, European journal of medicinal chemistry, 44 (2009) 954-958.

[47]. M. Gooshe, K. Ghasemi, M.M. Rohani, A. Tafakhori, S. Amiri, V. Aghamollaii, M. Ahmadi, A.R. Dehpour, Biphasic effect of sumatriptan on PTZ-induced seizures in mice: Modulation by 5-HT1B/D receptors and NOS/NO pathway, European journal of pharmacology, 824 (2018) 140-147.

[48]. F. Naaz, M.P. Pallavi, S. Shafi, N. Mulakayala, M.S. Yar, H.S. Kumar, 1, 2, 3-triazole tethered Indole-3-glyoxamide derivatives as multiple inhibitors of 5-LOX, COX-2 & tubulin: Their anti-proliferative & anti-inflammatory activity, Bioorganic chemistry, 81 (2018) 1-20.

[49]. W. Calhoun, R.P. Carlson, R. Crossley, L.J. Datko, S. Dietrich, K. Heatherington, L.A. Marshall, P.J. Meade, A. Opalko, R.G. Shepherd, Synthesis and Antiinflammatory Activity of Certain 5,6,7,8-Tetrahydroquinolines and Related Compounds, Journal of Medicinal Chemistry, 38 (1995) 1473-1481.

[50]. B. Bülbül, G.S. Öztürk, M. Vural, R. Şimşek, Y. Sarioğlu, A. Linden, M. Ülgen, C. Şafak, Condensed 1,4-dihydropyridines with various esters and their calcium channel antagonist activities, European journal of medicinal chemistry, 44 (2009) 2052-2058.

[51]. W. Zhu, X. Bao, H. Ren, Y. Da, D. Wu, F. Li, Y. Yan, L. Wang, Z. Chen, N-Phenyl indole derivatives as AT1 antagonists with anti-hypertension activities: design, synthesis and biological evaluation, European journal of medicinal chemistry, 115 (2016) 161-178.

[52]. S. Kumar, S. Bawa, H. Gupta, Biological Activities of Quinoline Derivatives, Mini-Reviews in Medicinal Chemistry, 9 (2009) 1648-1654.

[53]. W. Liu, H. Wang, X. Li, Y. Xu, J. Zhang, W. Wang, Q. Gong, X. Qiu, J. Zhu, F. Mao, Design, synthesis and evaluation of vilazodone-tacrine hybrids as multitarget-directed ligands against depression with cognitive impairment, Bioorganic & medicinal chemistry, 26 (2018) 3117-3125.

[54]. T.A. Halgren, Identifying and characterizing binding sites and assessing druggability, Journal of chemical information and modeling, 49 (2009) 377-389.

[55]. B. Li, F. Zhu, F. He, Q. Huang, X. Liu, T. Wu, T. Zhao, Y. Qiu, Z. Wu, Y. Xue, Synthesis and biological evaluations of N′-substituted methylene-4-(quinoline-4-amino) benzoylhydrazides as potential anti-hepatoma agents, Bioorganic Chemistry, 96 (2020) 103592.

[56]. P.F.M. Oliveira, B. Guidetti, A. Chamayou, C. Andre-Barres, J. Madacki, J. Kordulakova, G. Mori, B.S. Orena, L.R. Chiarelli, M.R. Pasca, C. Lherbet, C. Carayon, S. Massou, M. Baron, M. Baltas, Mechanochemical Synthesis and Biological Evaluation of Novel Isoniazid Derivatives with Potent Antitubercular Activity, Molecules, 22 (2017) 1457.

[57]. P.T. Tran, C.V. Phuong, P.H. Duc, D.T. Anh, P.T. Hai, L.T.T. Huong, N.T. Thuan, H.J. Lee, E.J. Park, J.S. Kang, N.P. Linh, T.T. Hieu, D.T.K. Oanh, S.B. Han, N.H. Nam, Novel 3,4-dihydro-4-oxoquinazoline-based acetohydrazides: Design, synthesis and evaluation of antitumor cytotoxicity and caspase activation activity, Bioorganic chemistry, 92 (2019) 103202.

[58]. L.C. Huan, C.V. Phuong, L.C. Truc, V.N. Thanh, H. Pham-The, L.T. Huong, N.T. Thuan, E.J. Park, A.Y. Ji, J.S. Kang, S.B. Han, P.T. Tran, N.H. Nam, (E)-N'-Arylidene-2-(4-oxoquinazolin-4(3H)-yl) acetohydrazides: Synthesis and evaluation of antitumor cytotoxicity and caspase activation activity, J Enzyme Inhib Med Chem, 34 (2019) 465-478.

[59]. V.T. Angelova, M. Rangelov, N. Todorova, M. Dangalov, P. Andreeva-Gateva, M. Kondeva-Burdina, V. Karabeliov, B. Shivachev, J. Tchekalarova, Discovery of novel indole-based aroylhydrazones as anticonvulsants: Pharmacophore-based design, Bioorg Chem, 90 (2019) 103028.

[60]. L. Zhang, F. Xie, J. Zhang, P. ten Dijke, F. Zhou, SUMO-triggered ubiquitination of NR4A1 controls macrophage cell death, Cell Death & Differentiation, 24 (2017) 1530-1539.

[61]. S. Perez-Sieira, M. Lopez, R. Nogueiras, S. Tovar, Regulation of NR4A by nutritional status, gender, postnatal development and hormonal deficiency, Scientific reports, 4 (2014) 4264.

[62]. T. Hazel, R. Misra, I. Davis, M. Greenberg, L. Lau, Nur77 is differentially modified in PC12 cells upon membrane depolarization and growth factor treatment, Molecular and cellular biology, 11 (1991) 3239-3246.

[63]. A. Pawlak, L. Strzadala, W. Kalas, Non-genomic effects of the NR4A1/Nur77/TR3/NGFIB orphan nuclear receptor, Steroids, 95 (2015) 1-6.

[64]. I. Tanida, N. Minematsu-Ikeguchi, T. Ueno, E. Kominami, Lysosomal Turnover, but Not a Cellular Level, of Endogenous LC3 is a Marker for Autophagy, Autophagy, 1 (2005) 84-91.

[65]. T.D. Evans, I. Sergin, X. Zhang, B. Razani, Target acquired: selective autophagy in cardiometabolic disease, Sci. Signal., 10 (2017) eaag2298.

[66]. N. Ohoka, S. Yoshii, T. Hattori, K. Onozaki, H. Hayashi, TRB3, a novel ER stress-inducible gene, is induced via ATF4–CHOP pathway and is involved in cell death, Embo Journal, 24 (2014) 1243-1255.

[67]. H. Hu, C. Lin, M. Ao, Y. Ji, B. Tang, X. Zhou, M. Fang, J. Zeng, Z. Wu, Synthesis and biological evaluation of 1-(2-(adamantane-1-yl)-1H-indol-5-yl)-3-substituted urea/thiourea derivatives as anticancer agents, RSC Advances, 7 (2017) 51640-51651.

[68]. C. Bodenreider, D. Beer, T.H. Keller, S. Sonntag, D. Wen, L.J. Yap, H.Y. Yin, S.G. Shochat, D. Huang, T. Zhou, A fluorescence quenching assay to discriminate between specific and nonspecific inhibitors of dengue virus protease, Analytical Biochemistry, 395 (2009) 195-204.

[69]. X. Chen, X. Cao, X. Tu, G. Alitongbieke, Z. Xia, X. Li, Z. Chen, M. Yin, D. Xu, S. Guo, BI1071, a novel Nur77 modulator, induces apoptosis of cancer cells by activating the Nur77-Bcl-2 apoptotic pathway, Molecular Cancer Therapeutics, 18 (2019) 886-899.

[70]. R.A. Friesner, J.L. Banks, R.B. Murphy, T.A. Halgren, J.J. Klicic, D.T. Mainz, M.P. Repasky, E.H. Knoll, M. Shelley, J.K. Perry, Glide: a new approach for rapid, accurate docking and scoring. 1. Method and assessment of docking accuracy, Journal of medicinal chemistry, 47 (2004) 1739-1749.

[71]. W. Sherman, T. Day, M.P. Jacobson, R.A. Friesner, R. Farid, Novel procedure for modeling ligand/receptor induced fit effects, Journal of medicinal chemistry, 49 (2006) 534-553.

[72]. R. Murphy, M. Repasky, Z. Zhou, R. Abel, G. Krilov, I. Tubert-Brohman, W. Sherman, R. Farid, R.A. Friesner, Evaluation of docking and scoring accuracy using a new version of Schrodinger's Glide XP and Induced Fit Docking (IFD) methodologies, in: ABSTRACTS OF PAPERS OF THE AMERICAN CHEMICAL SOCIETY, AMER CHEMICAL SOC 1155 16TH ST, NW, WASHINGTON, DC 20036 USA, 2011.

[73]. J.M. Swanson, R.H. Henchman, J.A. McCammon, Revisiting free energy calculations: a theoretical connection to MM/PBSA and direct calculation of the association free energy, Biophysical journal, 86 (2004) 67-74.

[74]. W. DeLano, The PyMOL Molecular Graphics System. DeLano Scientific; San Carlos, CA, USA: 2002, in, 2002.

Table 1. *In vitro* antiproliferative activities of the target compounds against liver cancer and normal cells

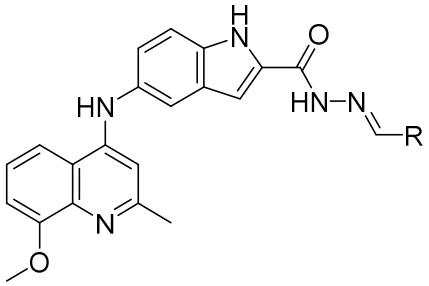

Compounds	R	IC_{50} (μM)[a]			
		HepG2	QGY-7703	SMMC-7721	LO2
10a	2-fluorophenyl	1.22±0.05[b]	5.42±1.34	1.38±0.23	2.48±0.44
10b	2-chlorophenyl	1.24±0.21	1.06±0.04	0.98±0.14	3.68±0.99
10c	2-methoxyphenyl	2.10±0.04	3.40±0.46	4.58±0.38	5.17±0.61
10d	3-methylphenyl	2.92±0.36	1.74±0.14	3.14±0.27	3.16±1.13
10e	3-methoxyphenyl	>20	>20	1.75±0.33	9.85±1.17
10f	3-(trifluoromethyl)phenyl	4.19±2.10	5.39±1.35	>20	13.54±3.03
10g	**4-(methylthio)phenyl**	**0.60±0.10**	**0.89±0.06**	**1.40±0.73**	**>20**
10h	4-methoxyphenyl	0.69±0.22	>20	1.21±0.48	0.76±0.22
10i	benzonitrile-4-yl	10.42±3.00	2.36±0.71	>20	2.80±0.82
10j	phenol-4-yl	>20	14.08±1.17	>20	9.31±2.80
10k	2,3-dimethoxyphenyl	1.09±0.19	1.96±0.26	4.89±0.89	2.79±0.40
10l	2,4-dihydroxyphenyl	8.15±3.50	>20	>20	15.93±1.76
10m	2,5-dihydroxyphenyl	>20	>20	>20	>20
10n	3,4-dimethoxyphenyl	>20	>20	>20	>20
10o	3-bromo-4-methoxyphenyl	>20	1.89±0.61	>20	1.20±1.10
10p	4-nitrophenol-2-yl	>20	>20	>20	>20
10q	2-bromo-5-(trifluoromethyl)phenyl	>20	12.74±1.90	>20	>20
10r	4-methoxy-3-(trifluoromethyl)phenyl	1.98±0.28	0.40±0.10	0.73±0.42	5.23±1.40
10s	4-fluoro-3-(trifluoromethyl)phenyl	2.17±0.90	2.43±0.56	>20	>20
10t	2,4-bis(trifluoromethyl)phenyl	>20	>20	>20	>20
10u	2,4-dimethoxyphenyl	7.47±1.00	5.00±0.82	16.21±1.51	5.72±1.30
10v	2,6-dimethoxyphenyl	7.52±0.21	>20	11.69±3.19	7.31±1.36
10w	3,5-dimethoxyphenyl	>20	>20	>20	>20
10x	2,3,4-trimethoxyphenyl	6.32±1.28	3.78±0.34	8.43±1.18	13.67±2.87
10y	3,4,5-trimethoxyphenyl	>20	>20	>20	>20
10z	3,5-di-tert-butyl-4-hydroxybenzyl-1-yl	7.45±1.41	4.02±0.73	>20	3.54±0.61
10A	1H-pyrrole-2-yl	>20	>20	>20	>20
10B	2-thiopheneyl	5.44±0.90	1.53±0.24	6.49±1.29	6.33±1.12
10C	2-pyridyl	14.74±3.64	>20	4.37±0.14	10.28±0.96

10D	3-pyridyl	>20	>20	>20	>20
10E	4-pyridyl	>20	>20	>20	>20
10F	4-methoxynaphthalen-1-yl	16.58±0.51	4.61±0.57	11.02±0.67	9.16±2.02
10G	quinoline-4-yl	>20	15.46±4.20	>20	>20
10H	2-chloroquinoline-3-yl	>20	9.31±0.60	18.80±1.64	>20
10I	5-methoxy-2-methyl-1H-indole-3-yl	6.62±1.01	14.13±1.22	>20	>20
PC1[c]	Celastrol	1.30±0.07	2.43±0.09	1.07±0.19	1.94±0.05
PC2[c]	CD437	2.93±0.91	2.38±0.11	5.25±2.17	10.08±1.39
PC3[c]	Cisplatin	7.22±1.36	6.23±1.34	5.24±0.92	16.00±2.33

[a] Cytotoxicity as IC_{50} for each cell line, is the concentration of compound which reduced by 50% the optical density of treated cells with respect to untreated cells using the MTT assay.

[b] Data are means ± SD of three independent determinations.

[c] Celastrol, CD437 and Cisplatin were taken as the positive controls.

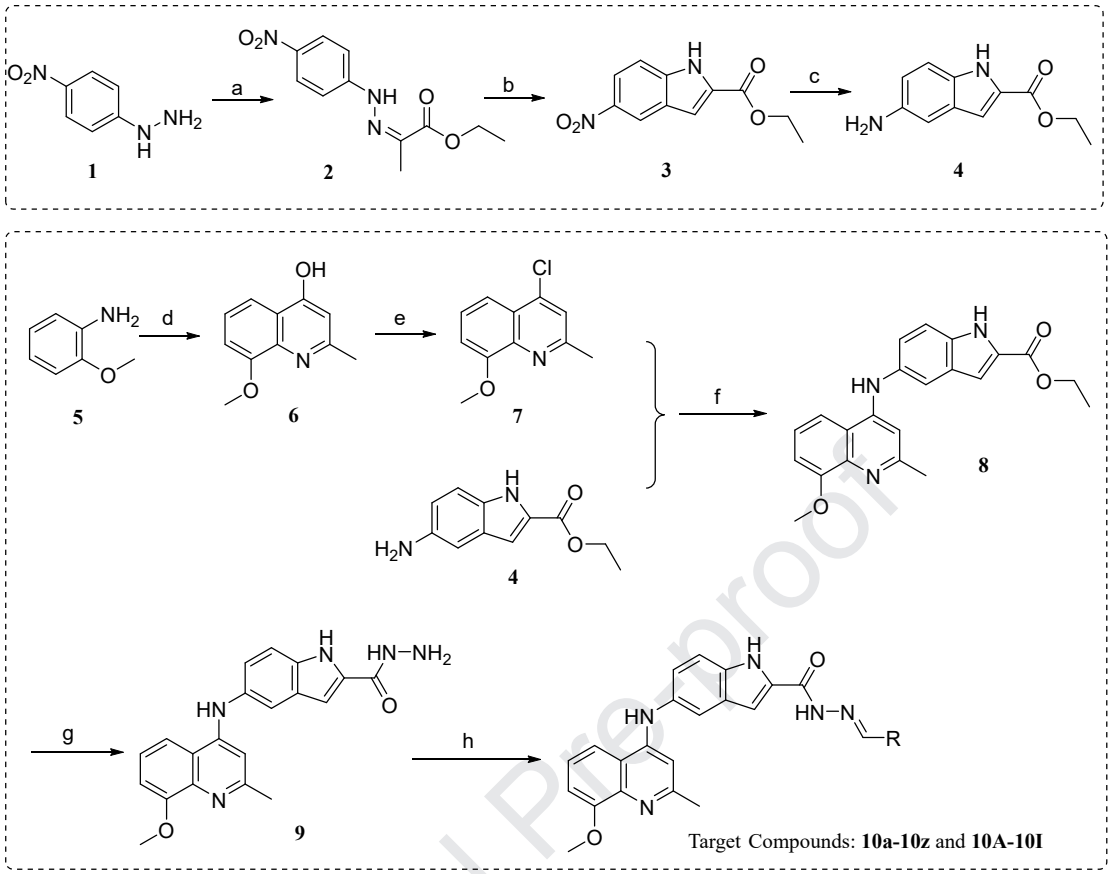

Scheme 1. Preparation of target compounds **10a-10z** and **10A-10I**. Reaction conditions: (a) Ethyl pyruvate, ethanol, reflux; (b) Polyphosphoric acid, 100℃, 2 h; (c) Fe, acetic acid aqueous, 70℃, 2 h; (d) Polyphosphoric acid, ethyl acetoacetate, 120℃; (e) $POCl_3$, 130℃; (f) 1-Butanol, concentrated hydrochloric acid, reflux; (g) Hydrazine hydrate, ethanol, reflux; (h) Ethanol, RCHO, trifluoroacetic acid, reflux.

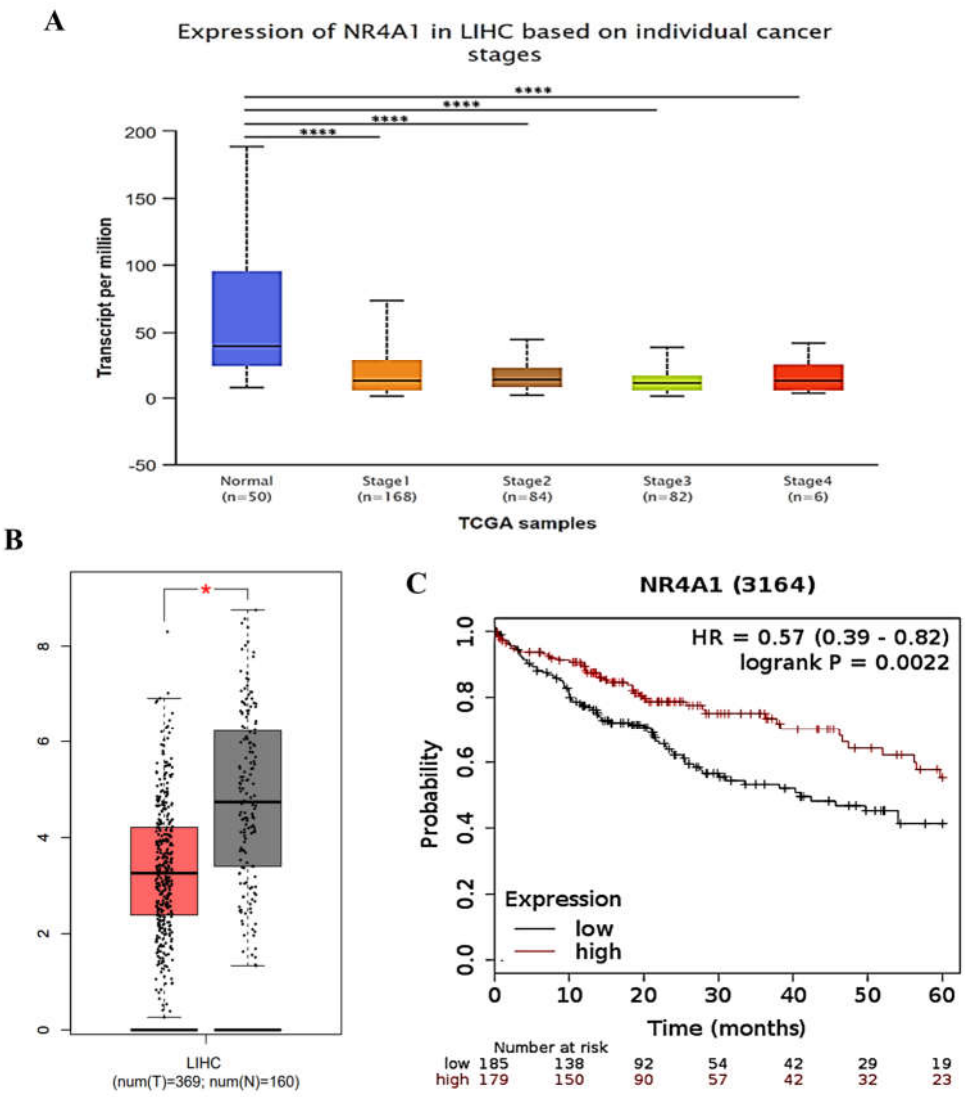

Figure 1. UALCAN and Kakaplan-meier analyses of Nur77 (NR4A1) in Hepatocellular carcinoma (LIHC). Box plot analysis of the immunoreactive score (IRS) of Nur77 (NR4A1) in 50 normal samples and 340 HCC samples grouped into stage I-IV with TCGA LIHC dataset(https://www.cancer.gov/). Nur77 expression is significantly down-regulated in LIHC. There are statistically significant differences in the expression level of Nur77 between normal tissues and tumor tissues of individual stages with a p-value less than 0.0001 (****) (**A**). Expression profiling of Nur77 in the Kakaplan-meier plotter database. Nur77 expression is significantly lower in tumor tissues than in the normal tissues. There are statistically significant differences in the expression level of Nur77 between tumor tissues and normal tissues with a p-value less than 0.05 (**B**). Kaplan-Meier survival curve shows the positive correlation between overall survival of HCC patients and Nur77 expression levels in 60 months from Kaplan-Meier Plotter dataset(http://kmplot.com/). Patients with Nur77 expression values below the 50th percentile are classified as lower Nur77 levels, while above the 50th percentile are classified as higher Nur77 levels. The median expression level was used as the cutoff. Survival information of 288 patients is available. HR (Hazards Ratio) =0.57, p(HR)=0.0022 (**C**).

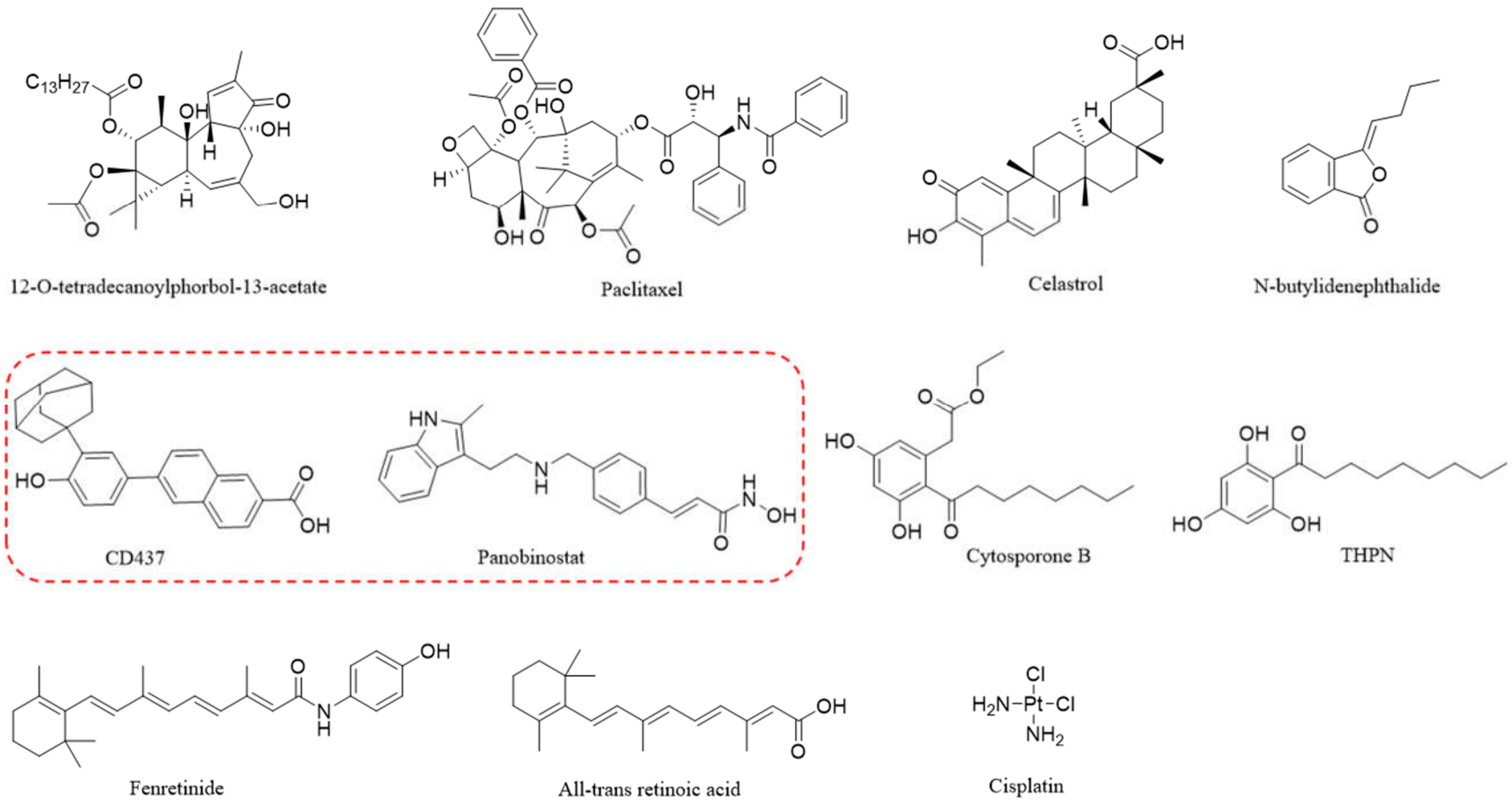

Figure 2. Chemical structures of representative Nur77 regulators

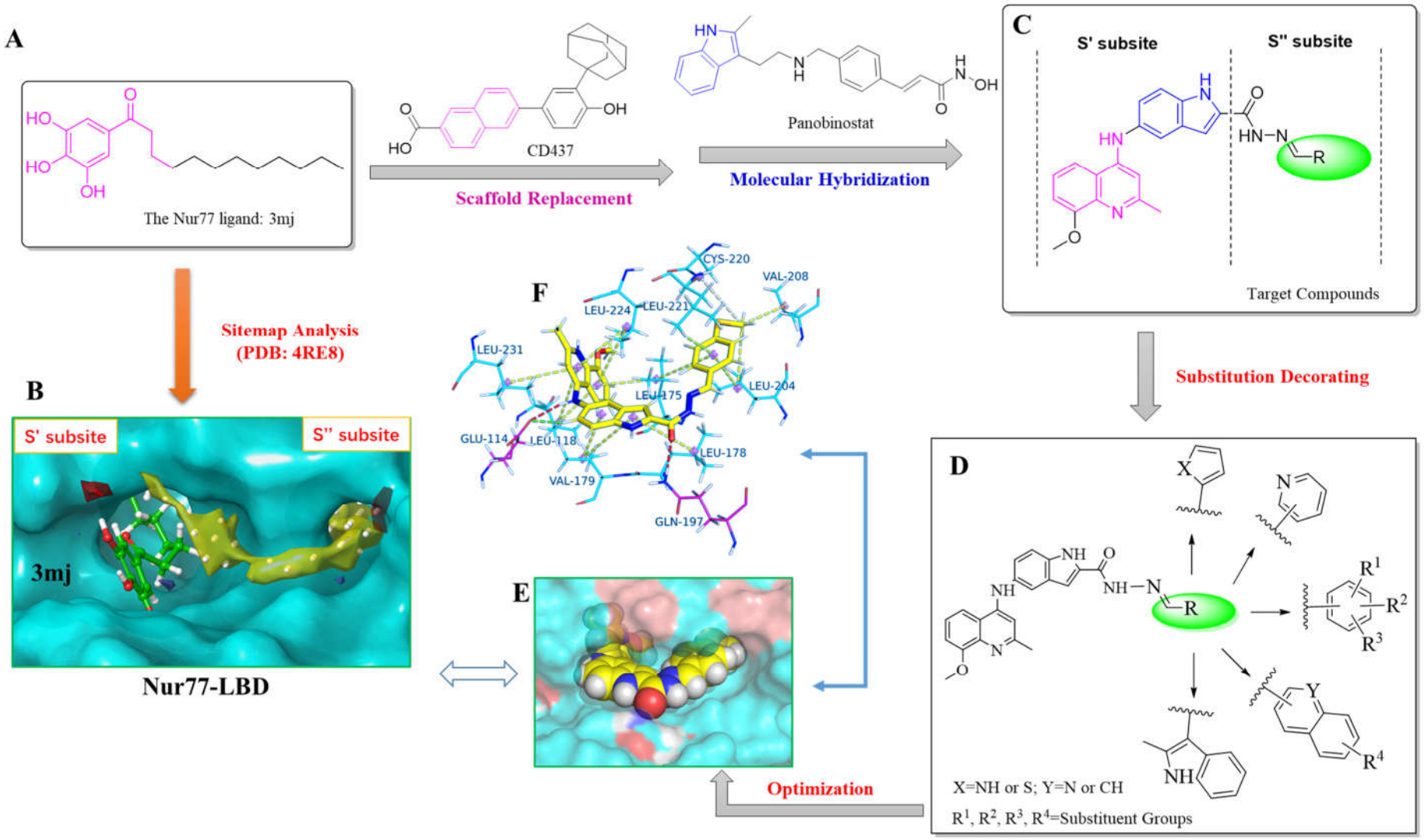

Figure 3. Design strategies used in our present study to obtain novel Nur77 regulators with 5-((8-methoxy-2-methylquinolin-4-yl)amino)-1*H*-indole scaffold.

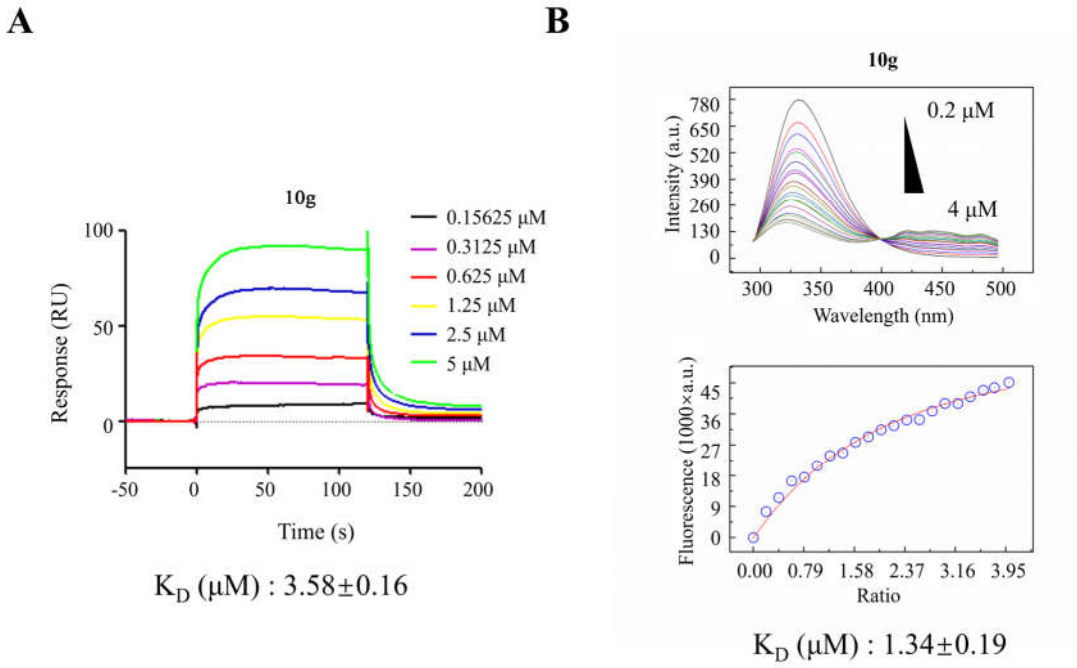

Figure 4. 10g bound directly to Nur77-LBD *in vitro*. Binding of **10g** to purified Nur77-LBD by SPR (**A**). Fluorescence titration curve of Nur77-LBD with **10g**. The concentration of **10g** increased from 0.2 μM to 4 μM at an interval of 0.2 μM (**B**).

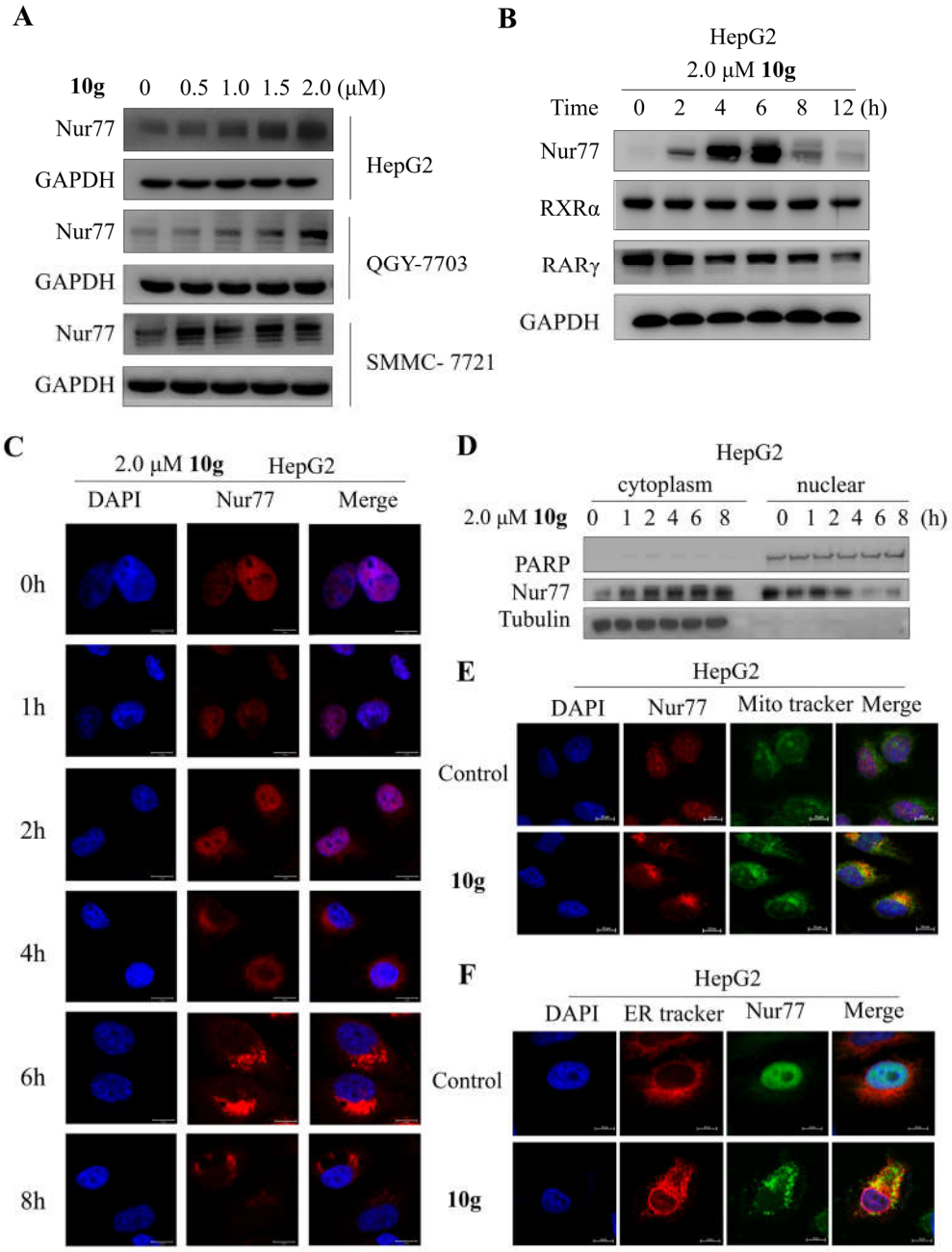

Figure 5. **10g** regulated expression and sub-cellular translocation of Nur77. HepG2, QGY-7703, and SMMC-7721 cells treated with the indicated concentration of **10g** for 6 hours were analyzed for Nur77 by western blotting GAPDH was used as an internal control (**A**). HepG2 cells were treated with 2.0 μM **10g** for indicated time. The expression of Nur77, RXRα and RARγ were detected by western blotting (**B**). Fluorescent images of HepG2 cells treated with 2 μM **10g** for indicated time and detected by Nur77. The nuclei were stained with DAPI. Scale bar, 10 μm. (**C**). HepG2 cells were treated with 2.0 μM **10g** for indicated time. Nur77 were detected in cytoplasm and nuclear by western blotting. PARP was used as an internal control of nucleus and Tubulin was used as an internal control of cytoplasm (**D**). HepG2 cells were treated with 2.0 μM **10g** for 6 hours and then incubated with Nur77 antibody and Mito-tracker (**E**) or ER tracker (**F**). Scale bar, 10 μm.

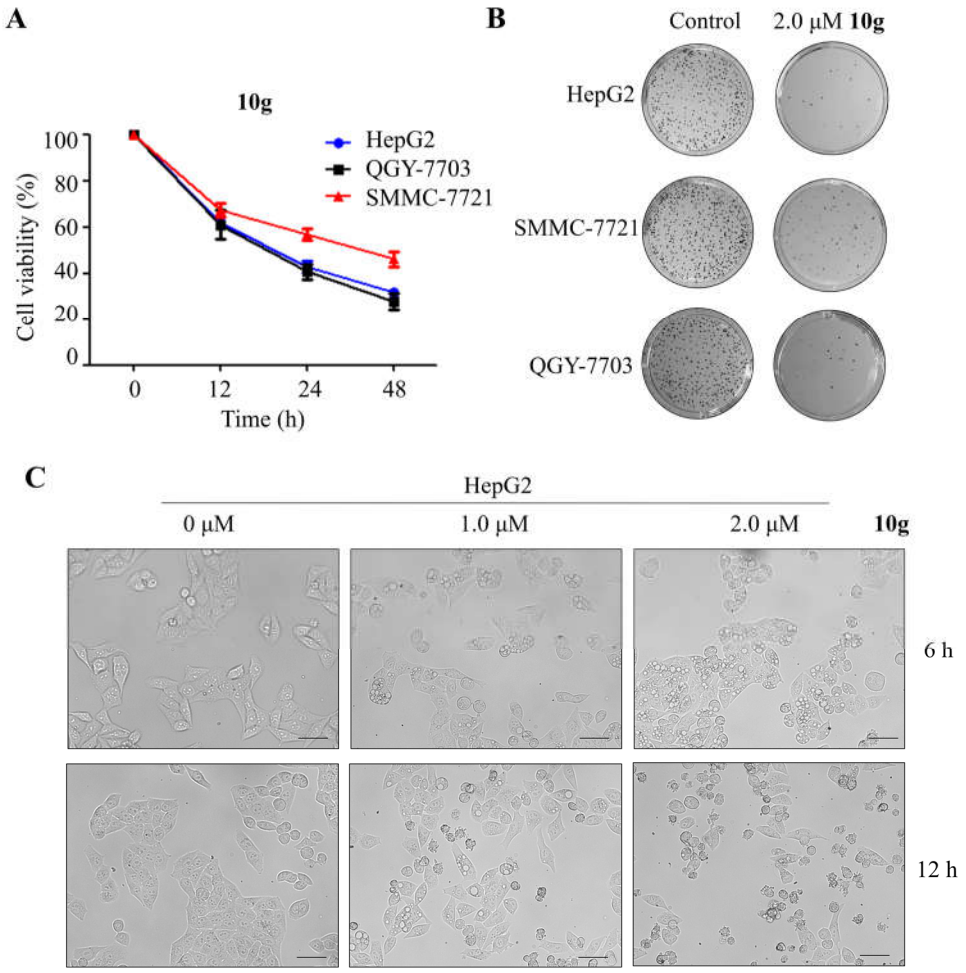

Figure 6. 10g inhibited the growth and proliferation of HCC. HepG2, QGY-7703, and SMMC-7721 cells were treated with 2.0 μM **10g** with the indicated time. Cell viability was determined by MTT assays (**A**). The number of colonies was counted after the treatment of HepG2, QGY-7703, and SMMC-7721 cells with DMSO or 2.0 μM **10g** (**B**). HepG2 cells were treated with **10g** at the indicated concentration, and the morphological changes were observed by optical microscopy at the indicated time (**C**).

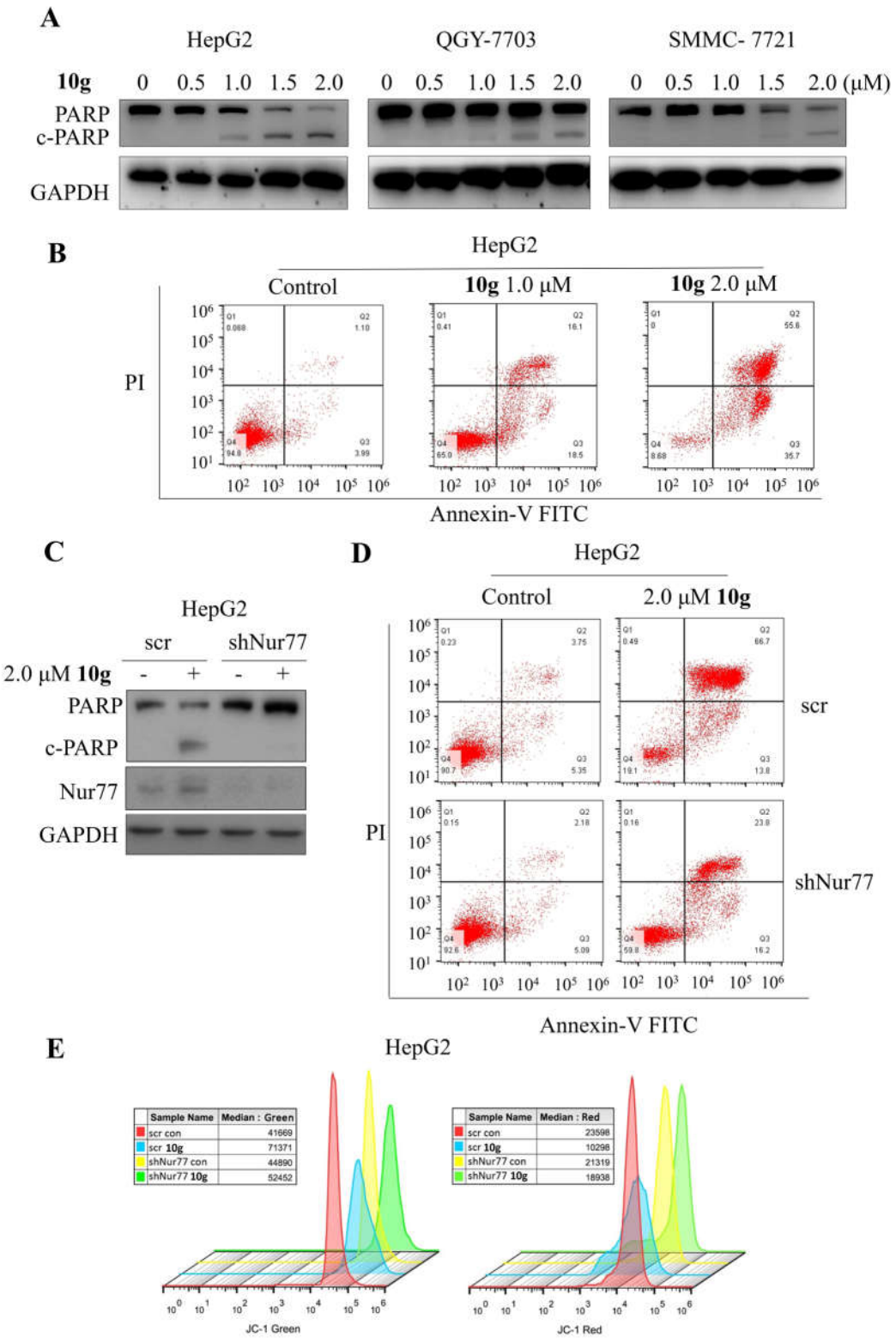

Figure 7. 10g induced Nur77-dependent apoptosis. Western blot analysis of proteins involved in apoptosis after treatment with **10g** at the indicated concentration for 12 hours in HepG2, QGY-7703, and SMMC-7721 cells (**A**). Annexin V/PI staining of HepG2 cells treated with **10g** at the indicated concentration for 12 hours and assessed by flow cytometry (**B**). HepG2 or shNur77 HepG2 cells were treated with 2 μM **10g** for 12 hours. Cells were then subjected to Western blotting for PARP cleavage and Nur77 detecting (**C**). Annexin V/PI staining for apoptosis measurement (**D**). JC-1 staining for mitochondrial membrane potential assay (**E**).

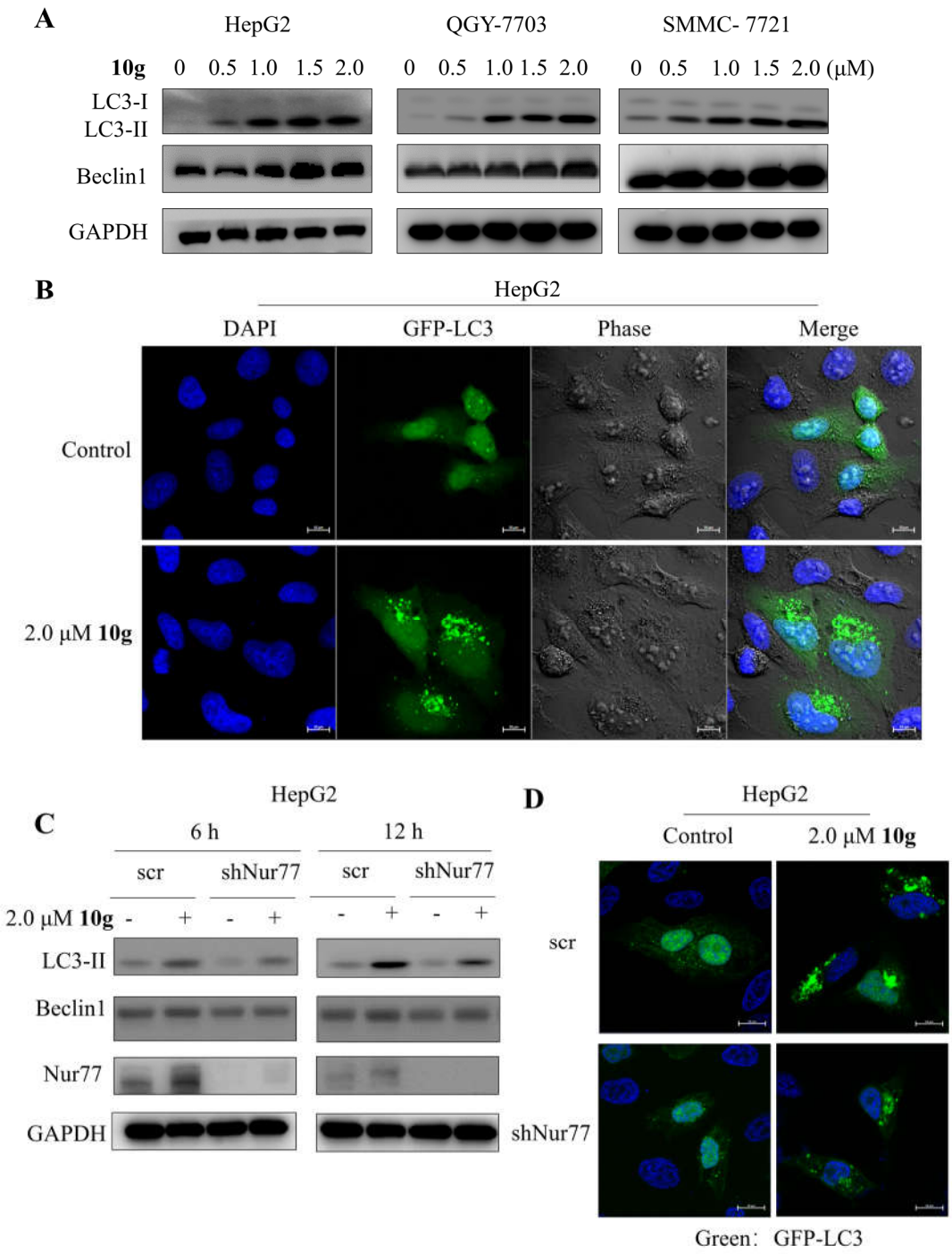

Figure 8. Induction of autophagy by **10g** in HCC. HepG2, QGY-7703, and SMMC-7721 were treated with **10g** at the indicated concentration for 12 h, the levels of LC3 and Beclin1 were detected by Western blotting (**A**). Phase-contrast and fluorescent images of HepG2 cells transfected with GFP-LC3 and treated with 2 μM **10g** for 6 hours. Scale bar, 10 μm (**B**). HepG2 or shNur77 HepG2 cells were treated with DMSO or 2 μM **10g** for 6 hours or 12 hours. Cells were then subjected to Western blotting for LC3, Beclin1, and Nur77 detecting (**C**). Fluorescent images of HepG2 and shNur77 HepG2 cells transfected with GFP-LC3 and treated with 2 μM **10g** for 6 hours. Scale bar, 10 μm (**D**).

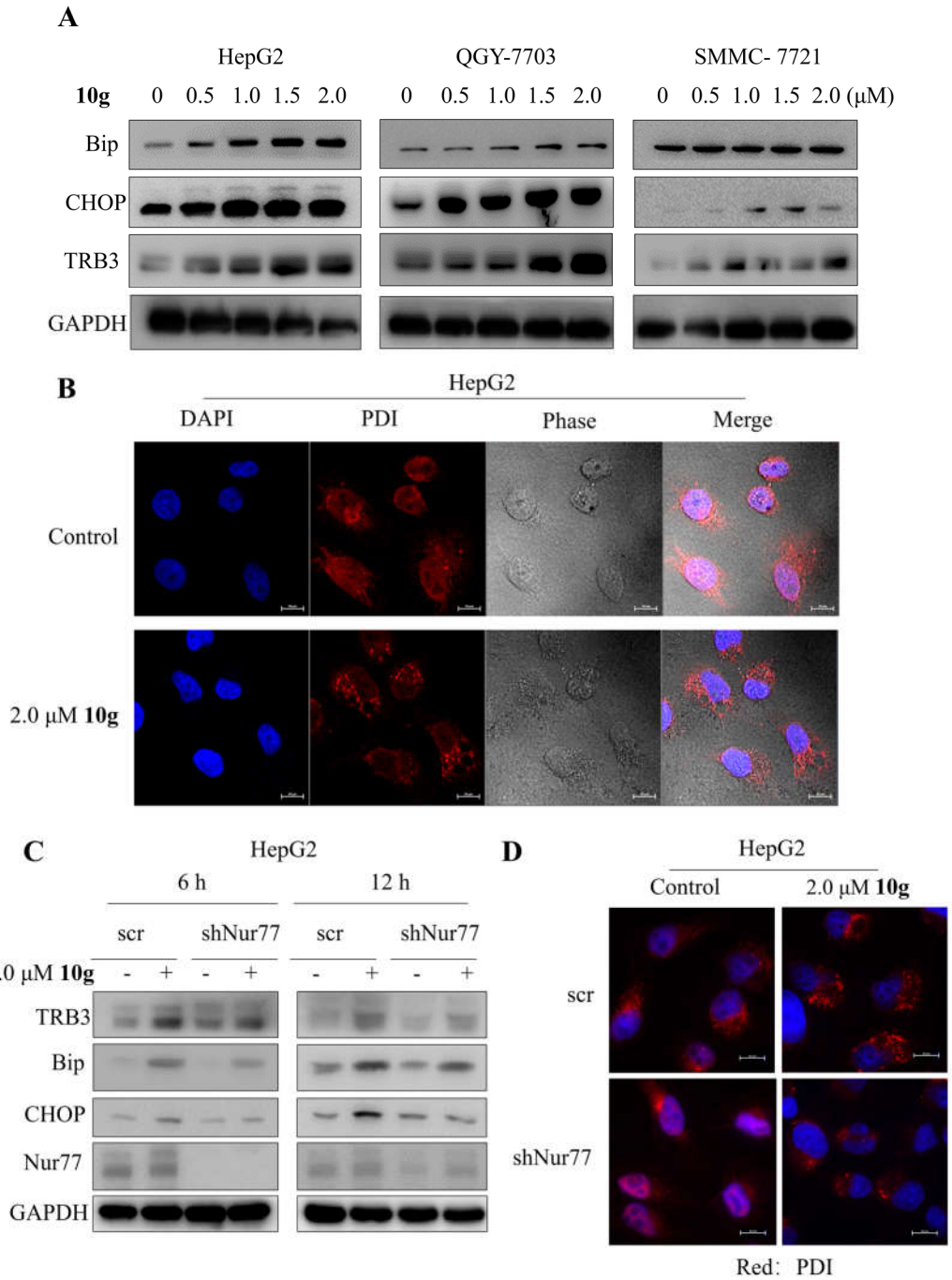

Figure 9. Induction of ER stress by **10g** in HCC. HepG2, QGY-7703, and SMMC-7721 were treated with **10g** at the indicated concentration for 12 h, the levels of Bip, TRB3, and CHOP were detected by western blotting (**A**). Phase-contrast and fluorescent images of HepG2 cells and treated with 2 μM **10g** for 6 hours and then incubated with PDI antibody. Scale bar, 10 μm (**B**). HepG2 or shNur77 HepG2 cells were treated with DMSO or 2 μM **10g** for 6 hours and 12 hours. Cells were then subjected to Western blotting for TRB3, Bip, CHOP, and Nur77 detecting (**C**). Fluorescent images of HepG2 and shNur77 HepG2 treated with 2 μM **10g** for 6 hours and then then incubated with PDI antibody. Scale bar, 10 μm (**D**).

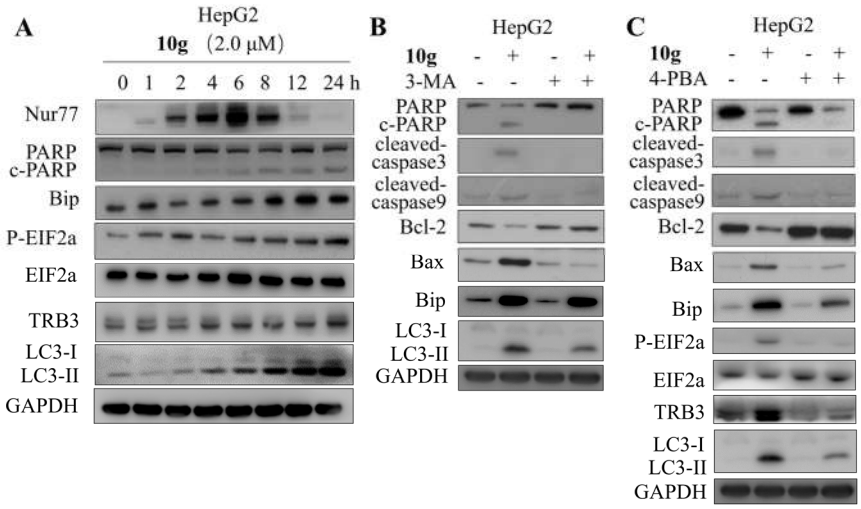

Figure 10. 10g induced apoptosis-dependent autophagic cell death mediated by ER-stress. HepG2 cells were treated with 2.0 μM **10g** for indicated time. The levels of autophagy associated proteins, ER stress-associated proteins, and Nur77 were detected by Western blotting (**A**). HepG2 cells were pretreated with 3-MA (2.0 mM) for 2 hours prior to exposure to **10g** for an additional 12 hours. Western blotting was performed to examine the levels of PARP, cleaved-caspase-3, cleaved-caspase-9, Bcl-2, Bax, Bip, and LC3(**B**). HepG2 cells were pretreated with 4-PBA (2.0 mM) for 2 hours prior to exposure to **10g** for an additional 12 hours. Western blotting was performed to examine the changes in protein levels of PARP, cleaved-caspase-3, cleaved-caspase-9, Bcl-2, Bax, Bip, EIF2a, TRB3, and LC3(**C**).

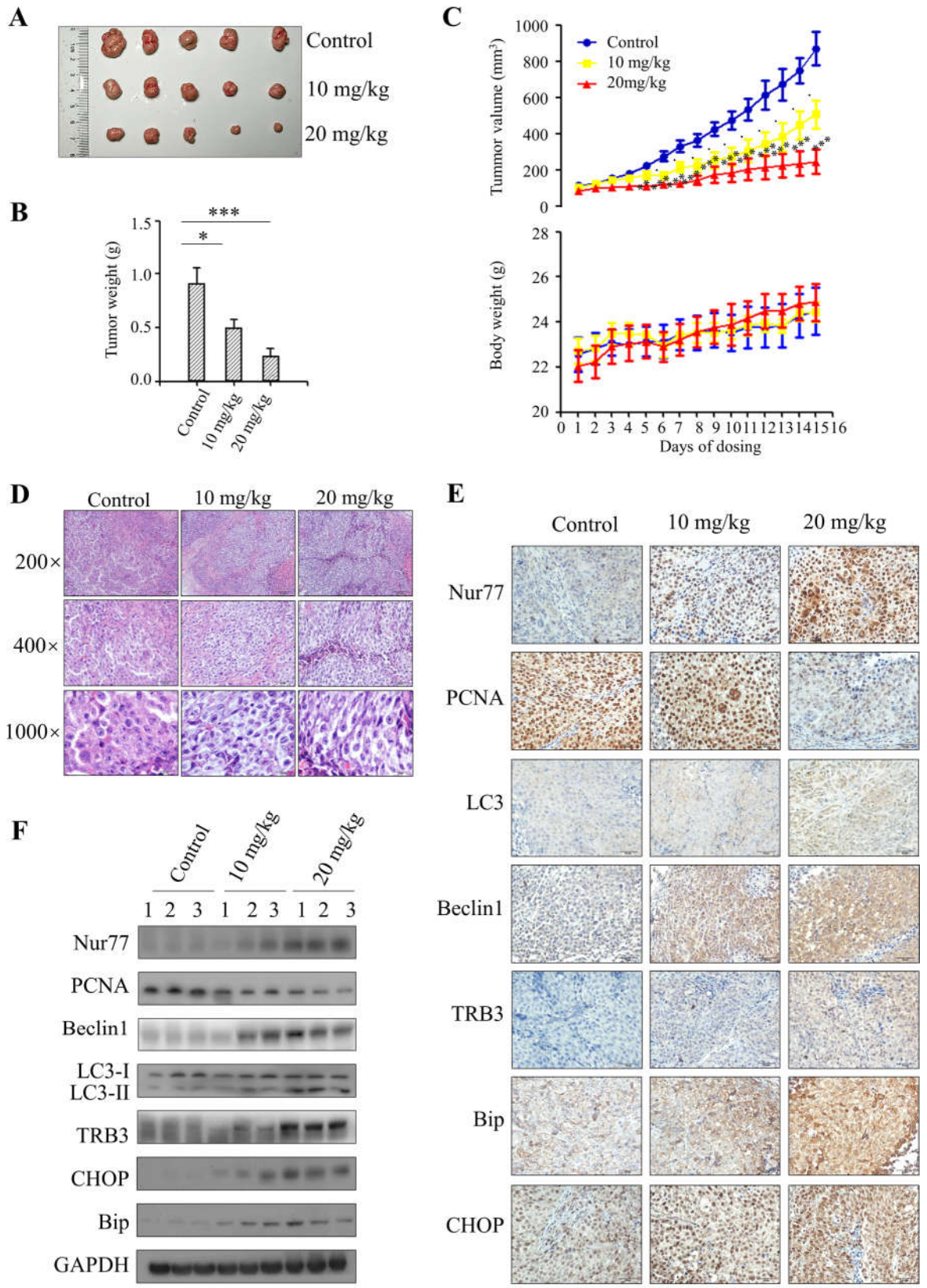

Figure 11. 10g exhibited in vivo efficacy in a xenograft mouse model of HepG2 cells. Nude mice (n=15) injected with HepG2 (5×10^6 cells) were administrated with the indicated dose of **10g** (10 mg/kg; 20 mg/kg) once a day and tumors were measured every day. 15 days after administration of **10g**, nude mice bearing HepG2 tumors were sacrificed and tumors were removed, weighted and showed (***P< 0.001, **P< 0.01, *P< 0.05) (**A, B**). Tumor volume and body weight of nude mice during treatment (***P< 0.001, **P< 0.01, *P< 0.05, ·P< 0.05) (**C**). H&E staining in tumors untreated or after 15 days of treatment with **10g** (**D**).

Micromagnification was 200, 400, and 1000 times respectively. Immunocytochemistry staining showing the expression of Nur77, PCNA, LC3, Beclin1, TRB3, Bip, and CHOP in tumor tissues prepared from nude mice treated with or without **10g** (10 mg/kg; 20 mg/kg) for 15 days (**E**). Western blot analysis of the expressions of Nur77, PCNA, LC3, Beclin1, TRB3, Bip, and CHOP in tumor tissues prepared from nude mice treated with or without **10g** (10 mg/kg; 20 mg/kg) for 15 days (**F**).

Synthesis, and Biological Evaluation of 5-((8-Methoxy-2-Methylquinolin-4-yl)Amino)-1*H*-Indole-2-Carbohydrazide Derivatives as Novel Nur77 Modulators

Baicun Li[1, 2, #], Jie Yao[1, #], Kaiqiang Guo[1,#], Fengming He[1], Kun Chen[1], Zongxin Lin[1], Shunzhi Liu[1], Jiangang Huang[1], Qiaoqiong Wu[1], Meijuan Fang[1,*], Jinzhang Zeng[1,*], Zhen Wu[1,*]

Highlights:

- Compound **10g** is a good binder of Nur77 (K_D = 3.58±0.16 μM).
- **10g** exhibits good anti-hepatoma activity and low toxic to LO2 cells.
- **10g** up-regulates Nur77 expression and mediates sub-cellular localization of Nur77.
- **10g** induces apoptosis mediated by Nur77-dependent ER stress and autophagy.
- **10g** inhibits tumor growth in a mice hepatoma HepG2 xenograft model.

Declaration of Competing Interest

Authors have no conflict of interest to declare.